Schweizerische Eidgenossenschaft
Confédération suisse
Confederazione Svizzera
Confederaziun svizra

Department of the Environment, Transport, Energy and Communication DETEC

Swiss Federal Office of Energy SFOE
Energy Research

Final report dated 13.12.2019

OPTSAIS – Exergetic and Economic Optimization of Seasonal Thermal Energy Storage Systems

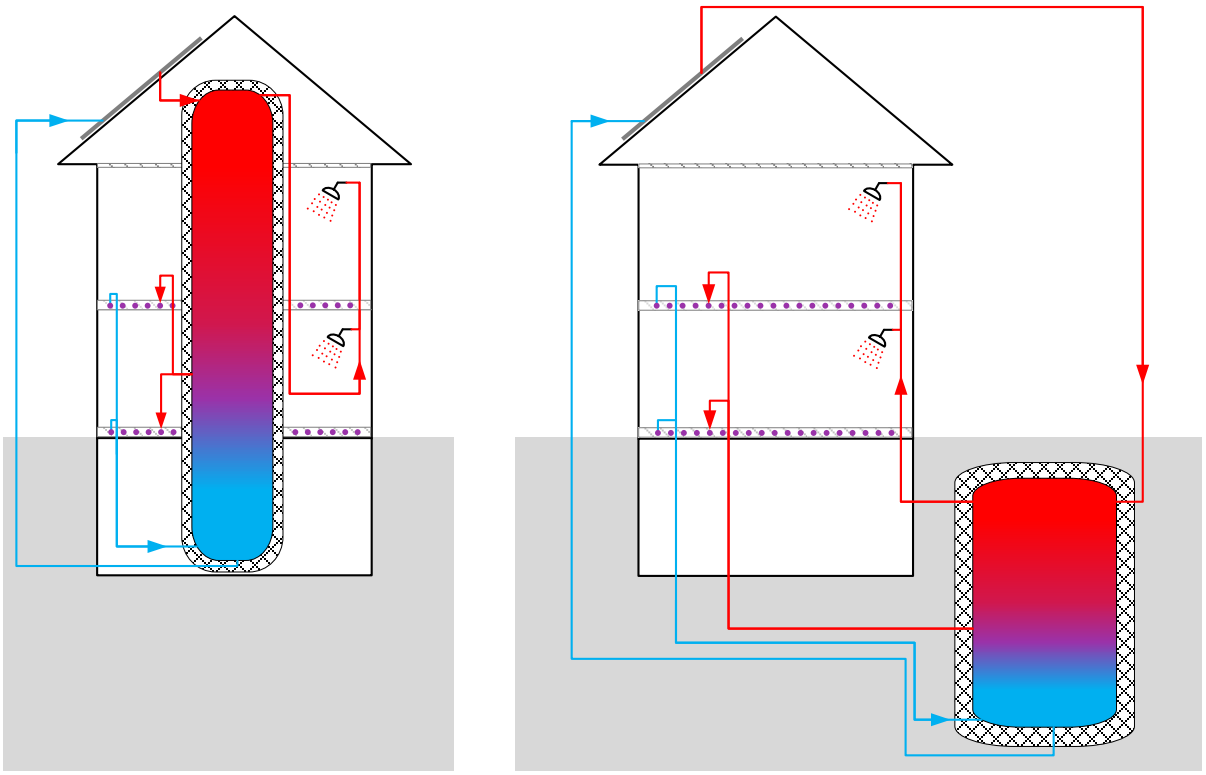

Source: HSLU

Lucerne University of
Applied Sciences and Arts

HOCHSCHULE
LUZERN

HOCHSCHULE LUZERN
THERMAL ENERGY STORAGE

Date: 13. December 2019

Location: Horw

Publisher:
Swiss Federal Office of Energy SFOE
Section Energy Research
CH-3003 Bern
www.bfe.admin.ch

Subsidy recipient:
Hochschule Luzern – Technik und Architektur
Competence Center Thermal Energy Storage
Technikumstrasse 21
CH-6048 Horw
www.hslu.ch/tes

Authors:
Willy Villasmil, Hochschule Luzern, willy.villasmil@hslu.ch
Marcel Troxler, Hochschule Luzern, marcel.troxler@hslu.ch
Reto Hendry, Hochschule Luzern, reto.hendry@hslu.ch
Jörg Worlitschek, Hochschule Luzern, joerg.worlitschek@hslu.ch

SFOE project coordinators:
SFOE head of domain: Andreas Eckmanns, andreas.eckmanns@bfe.admin.ch
SFOE program manager: Elimar Frank, elimar.frank@frank-energy.com

SFOE contract number: SI/501565-01

Summary

In combination with seasonal thermal energy storage (STES), solar energy offers a vast potential for the supply of space heating and domestic hot water. Today, increasing market diffusion of STES requires reducing the high investment costs. In this work, a parametric-based optimization is conducted to assess the potential of reducing the costs of hot-water STES through the use of alternative thermal insulation materials and an exergy-oriented control strategy of the solar collectors. The investigated configurations include: (1) a hot-water thermally stratified storage, (2) a solar thermal collector installation, and (3) a representative multifamily low-energy building with a solar fraction of 100%. The storage tank is either integrated inside the building (either new building or retrofit) or buried underground in direct vicinity of the building.

A simulation-based analysis shows that the required storage volume can be reduced by 30% by switching from a high-flow (baseline case) to a low-flow control strategy – this for a typical tilt angle of the solar collectors of 45°. If the tilt angle is increased to an optimum of 65°, the storage volume can be further reduced by round 10%. If the hot-water tank is integrated as part of a retrofitting inside an existing residential building – where the costs are primarily driven by the loss of living space –, maximizing the solar collector area is the best strategy to minimize the Levelized Cost of Energy Storage ($LCOES_{100}$). In the retrofitting scenario, vacuum-insulation panels (VIP) – as an alternative to conventional glass wool – can lead to 20% savings in living space and a cost advantage of about 5%. At an $LCOES_{100}$ of about 1.1 CHF/kWh, the integration of the storage inside an existing building is the most expensive option due to the high costs associated to the internal modification of the building and the loss of living space. The $LCOES_{100}$ can be reduced by 50% if the storage is integrated inside a new building – mainly because of the high building reconstruction costs that are avoided. If the regulations would allow the storage to be removed from the calculation of the building footprint (in German the so-called 'Ausnützungsziffer'), the $LCOES_{100}$ could be further reduced by 40%, reaching a minimum of 0.4 CHF/kWh. In spite of the high excavation costs and the increased heat losses, the concept of burying the STES underground – in direct vicinity of the building – represents a promising option ($LCOES_{100}$ ~0.6 CHF/kWh) to allow the integration of seasonal storage system in both new and existing residential buildings.

In this study, the focus was on residential buildings with solar fractions of 100%. It is envisaged that the economic optimum of future energy systems will be reached at lower autarky levels and bigger systems that include multiple buildings that make use of sector coupling strategies – e.g. by using photovoltaic installations in combination with heat pumps.

Table of contents

Nomenclature

Symbols

A	$[\mathrm{m}^2]$	Area
A_{sol}	$[\mathrm{m}^2]$	Total area of the solar thermal collector installation
A_{TES}	$[\mathrm{m}^2]$	Total cross-sectional area of the storage (tank plus thermal insulation)
c	$[\mathrm{J/m^2K}]$	Effective thermal capacity of the building per m^2 wall
c_p	[J/kg K]	Specific heat capacity
C	[J/K]	Effective thermal capacity of the building
E	[J]	Energy
F_{frame}	$[-]$	Frame factor
g	$[\mathrm{m}^2]$	Gain factor
h	$[\mathrm{W/m^2K}]$	Convective heat transfer coefficient
H	[W/K]	Heat loss factor
I	$[\mathrm{W/m}^2]$	Solar irradiance
$k_{\mathrm{VK,AF}}$	[CHF/a]	Annual full cost
m	[kg]	Mass
$\dot{m}$	[kg/s]	Mass flow rate
N	$[-]$	Amount
$\dot{Q}$	[W]	Power
r	[m]	Radius
Re	$[-]$	Reynolds number
t	[s]	Time
T	[K]	Temperature
u	[m/s]	Velocity
U	$[\mathrm{W/m^2K}]$	Overall heat transfer coefficient
V_{tank}	$[\mathrm{m}^3]$	Effective storage volume
V_{TES}	$[\mathrm{m}^3]$	Total volume of the storage (V_{tank} + volume of the thermal insulation)
W	[kWh/a]	Annual energy output of the storage
z	[m]	Distance

Greek symbols

δ	[m]	Thickness
λ	[W/mK]	Thermal conductivity
ρ	$[\mathrm{kg/m}^3]$	Density
η_0	$[-]$	Efficiency parameter (solar collector model)

Indices

amb	Ambient
coll	Collector
com	Component
const	Construction
crit	Critical
exc	Excavation
ext	Extern
gly	Glycol
heat	Heating
i	Inside
imo	Real estate (living space)
in	Inlet
ins	Insulation
inst	Installation
int	Intern
max	Maximum
min	Minimum
o	Outside
out	Outlet
req	Required
sol	Solar
STO	Storage
targ	Target
w	Water

Acronyms

ANF	Annuity factor
CAPEX	Capital expenditure
DHW	Domestic hot water
GW	Glass wool
HEX	Heat exchanger
HFC	High flow controller
HTF	Heat transfer fluid
$LCOES_{100}$	Levelized cost of energy storage with 100% autarky
LFC	Low flow controller
MFC	Matched flow controller
NB-FA	New building, footprint affected
NB-FU	New building, footprint unaffected
OPEX	Operational expenditure
PIR	Polyisocyanurate
POR	Port
RF	Retrofit
SH	Space heating
STES	Seasonal thermal energy storage
TES	Thermal energy storage
TRL	Technology readiness level
VES	Vessel
VIP	Vacuum insulation panel
XPS	Extruded polystyrene

1 Introduction

Seasonal thermal energy storage is an important technology for the Swiss Energy Strategy 2050 [1]. The evaluation panel of SCCER has emphasized the importance of integrating cost-effective seasonal thermal energy storage in the Swiss building sector. In combination with thermal energy storage, renewable energy technologies offer a vast potential for the supply of residential space heating (SH) and the production of domestic hot water (DHW). In 2014, the final energy consumption for SH and hot water amounted to round 254 PJ, which is about one third of the Swiss final energy consumption [2]. More than one million buildings in Switzerland are in need of renovation [3] and 64% of residential buildings are heated with fossil fuels. More than 70% of multifamily houses are heated with fossil fuels [4] and emit about 40% of the carbon dioxide of the entire building stock [3]. Single-family houses account for 27% of CO_2 emissions [3]. In Switzerland, it is estimated that a total solar coverage of the annual heat demand would be possible in more than 30% of multifamily residential buildings [5].

In a study on the solar heat potential in Switzerland [6], Gutschner et al. show that a completely solar coverage of the energy demand for space heating and domestic hot water in 58% of single-family houses and 40% of multifamily houses in the canton of Fribourg can hypothetically be achieved. In the city of Zürich, 40% of single-family houses and 9% of multifamily houses can theoretically be completely heated by solar energy. The study assumes specific energy consumption of 30 kWh/a for space heating and optimal seasonal heat storage. Throughout Switzerland, the proportion of buildings whose heating requirements can theoretically be covered entirely by solar energy is likely to be at a similar level.

Sensible, seasonal solar heat storage systems have already been implemented in various projects in Switzerland. One example is the solar houses in Oberburg (BE) [7] with storage volumes in the range 100 – 200 m^3. As Hewickler et al. [1] and Mangold et al [8] show, the specific investment costs per storage capacity for storage facilities of this size are higher than for storage facilities of ten to one hundred times greater capacity. This is why storage facilities of this size are used only sporadically today. It is therefore important to drive forward volume reduction so that the technology can gain a foothold in the market even under the current cost conditions.

The problem of reaching an increased market diffusion of STES is not attributed to a lack of knowledge of these technologies, which is considered to be high, but rather to their high cost [9]. Particularly in the case of hot-water STES, it becomes of paramount importance to minimize the annual heat losses while ensuring the economic feasibility of the storage system. These conflicting requirements lead to an optimization problem in which the costs of the insulation system and the storage container need to be balanced against the penalty costs associated to the annual heat losses and the space occupied by the storage system. The latter is particularly important when the storage is placed inside a residential building.

In this work, a parametric-based optimization is conducted to assess the potential of reducing the costs of hot-water STES through the use of alternative thermal insulation materials and an exergy-oriented control strategy of the solar collectors. The investigated configurations include the hot-water storage, a series of solar thermal collectors, and a representative building with a solar fraction of 100%.

2 Scenarios and system description

The investigated configurations include: (i) a hot-water thermally stratified seasonal thermal energy storage, (ii) a solar thermal collector installation, and (iii) a representative residential multifamily building with a solar fraction of 100%. Two scenarios are considered in this work (see Fig. 1): (1) a storage tank integrated inside the building, and (2) a storage tank buried underground in direct vicinity of the building. The maximum storage temperature is limited to 90 °C.

Scenario 1 involves the application of thermal insulation materials on the outside of the storage. Thermophysical properties and costs of conventional materials (such as mineral wools) are compared against those of state-of-the-art products such as VIP. A parametric comparative analysis is conducted to evaluate the combined costs of thermal insulation and living space occupied by the thermal insulation for STES systems integrated inside buildings. It is shown, for example, that the use of VIP becomes advantageous when the economic value of saving living space outweighs the extra cost of VIP itself. Scenario 2 requires the use of so-called evacuated powders, in which the insulation is realized by creating an evacuated double-wall powder-containing envelope around the storage.

2.1 Scenarios

Two different scenarios for a predefined reference building are examined. The scenarios differ mainly in the location of the storage and the thermal insulation used.

Scenario 1 - Storage integrated inside the building

In this scenario, the storage consists of a cylindrical steel tank placed inside the building in a shaft. The shaft is arranged centrally in the building and extends from the basement over several floors to the top of the building. The steel tank is insulated with one of the following materials: glass wool (GW), extruded polystyrene (XPS), polyurethane-polyisocyanurate foam (PUR-PIR) or VIP. A major disadvantage of this scenario is the loss of living space (and the associated cost penalties) that results from placing the storage inside the building. This storage concept is offered by the Swiss company Jenni Energietechnik AG, who has already implemented this system in several houses in and outside Switzerland [10,11]. In this study, three different cases have been considered:

- **Retrofit:** Integration of the STES system in an existing building. The loss in living space and the need for an internal reconstruction of the building translates into large penalty costs.
- **New building, footprint affected**: The STES system is integrated in a new building. In this case, the space occupied by the tank counts as part of the building footprint[1] (in German the so-called 'Ausnützungsziffer'). The reduction in the available footprint translates into a penalty cost.
- **New building, footprint unaffected**: The STES system is integrated in a new building. The space occupied by the tank does not count as part of the building footprint. This is the ideal case for this scenario, as no penalty costs result from integrating the storage inside the building.

In scenario 1, the building is also heated directly by means of the heat losses of the storage tank. Given that this additional heating is not controlled, the building is further heated in summer.

Scenario 2 - Storage buried underground

A vacuum-insulated steel tank is buried underground in direct vicinity of the building. The thermal insulation is realized by means of a vacuum that is generated between the inner and outer tank shell. The evacuated envelop is further filled with small particles with the aim of suppressing radiative heat transfer (see Section 2.4). As of today, at least two companies offer this storage concept in the market [12,13].

[1] The building footprint is the ratio between the eligible gross floor area of the building and the eligible land area [64].

2.2 System description

The investigate system comprises three sub-systems, each of them controlled in close interaction: (1) thermal energy storage, (2) solar thermal collectors, (3) building.

Thermal energy storage

The storage medium of the thermal energy storage (TES) system is water up 90°C. The tank configuration, shown schematically in Fig. 2, contains four helical heat exchangers (HEX 1-4), three internal vessels for domestic hot water (VES 1-3) and four ports (POR 1-4). The HEXs are connected with the solar thermal collector's circuit to allow the solar energy absorbed by the collectors to be transferred to the storage medium inside the tank. HEXs and VESs are hermetically separated from the storage medium. The ports allow the water in the tank to be circulated through the space heating system of the building. POR 1 is an inlet (return from the SH system), POR 2-4 are outlets.

Solar thermal collectors

The solar thermal collector installation is considered the only external heat source. They are allowed to operate up to 110°C based on the temperature of the heat transfer fluid (HTF) at the outlet of the collectors. The HTF is considered a mixture of 60 vol% water and 40 vol% Glythermin P44. The absorbed solar energy is then transferred to the storage by means of the helical heat exchangers placed inside the storage tank – the latter denoted by 'HEX' in Fig. 2.

Building

The building simulates the heat demand depending on its geometry, window area, number of rooms, etc. The heating demand is supplied via a floor heating emitter system directly connected to the storage.

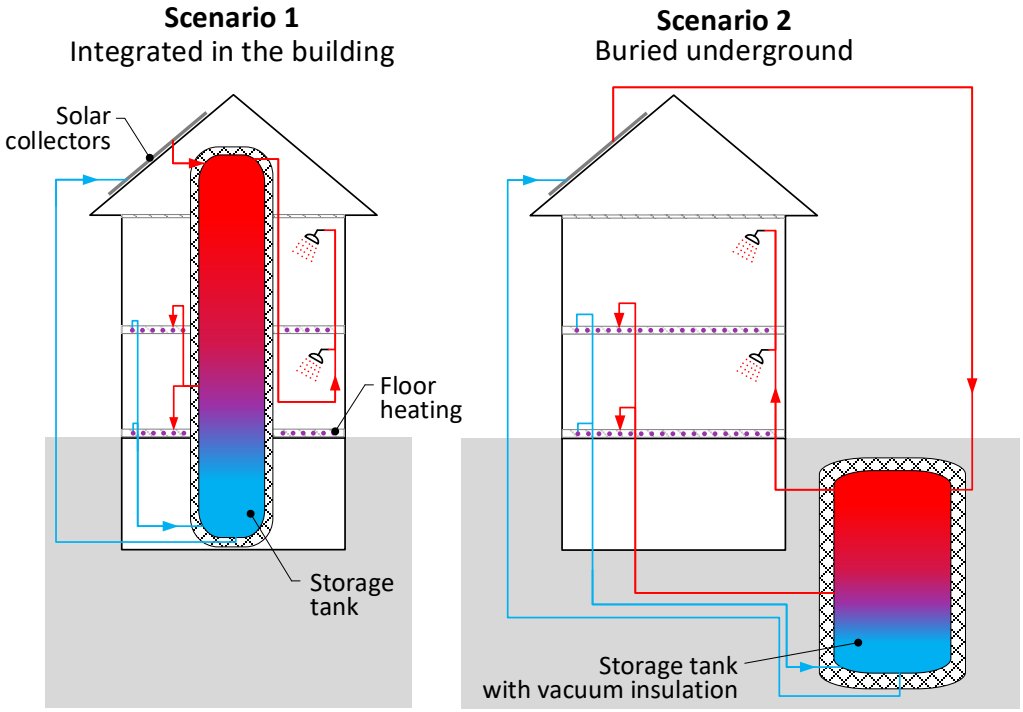

Fig. 1 – Considered scenarios. Left: storage integrated inside the building, Right: vacuum-insulated storage buried underground in direct vicinity of the building. The only external heat source are the solar collectors.

2.3 Operating principles

2.3.1 Solar collector control strategy

The solar collector control strategy has a major influence on the solar yield and particularly on the thermal stratification attained in the storage tank. In this work, the solar collector circuit is controlled through a passive or active variation of the HTF mass flow rate. Low flow rates allow higher temperatures to be achieved at the outlet of the solar collector (higher exergy efficiency), however at the expense of increased thermal losses. Higher flow rates allow harvesting more solar energy due to the increased energy efficiency, however at the expense of delivering the HTF at lower temperatures. Thus, the challenge translates into tuning the controller such the ideal compromise between energy and exergy efficiency is found. The following three control strategies are investigated in this work.

Here, it is assumed that the cost differences that result from changing the controller (e.g. those associated to the control hardware and software, the circulation pump and piping of the solar circuit) are negligible compared to all other investment costs associated to the storage, solar collectors, etc. The difference in electricity consumption of the circulation pump in the solar circuit is also disregarded in this analysis. The costs associated to the electricity consumption are included in the assumed operational expenditure (see Section 5.2.1).

High Flow

Today, high flow control (HFC) is the most common method used to control a solar thermal installation for seasonal thermal energy storage applications. With HFC, the HTF circulation pump is not actively controlled, but runs at a constant speed regardless of the solar irradiation conditions and the state of charge of the storage. For a given pump and piping configuration, the HTF flows through the solar collectors at a flow rate that solely depends on the pressure loss in the solar circuit. In this study, a specific flow rate of 40 l/m^{2}h is used as reference value [14].

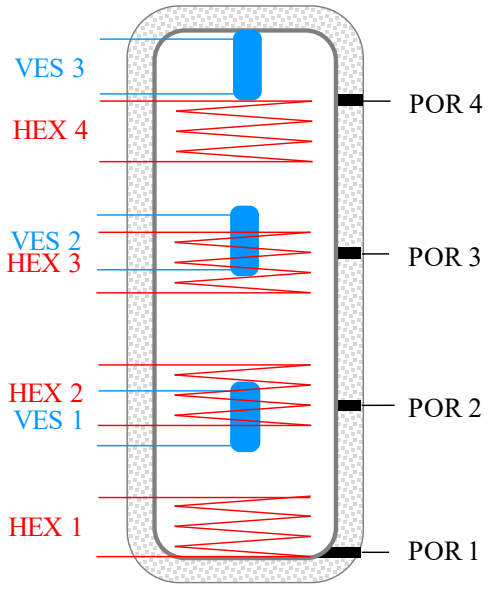

Fig. 2 – Arrangement of the HEX, VES and POR in the storage. **HEX** (see Fig. 4): the heat exchangers allow the energy harvested by the solar collectors to be transferred to the storage medium (water) in the tank. **VES** (see Fig. 5): vessels for heating domestic hot water. **POR** (see Fig. 6): the ports allow the hot water from the tank to be circulated through the building's heating system.

Low Flow

With low flow control (LFC), the HTF circulation pump is not actively controlled, but runs at a constant speed regardless of the solar irradiation and the state of charge of the storage. A specific flow rate of 12.5 l/m²h is used as reference value in this work [14].

Matched Flow

With matched flow control (MFC), the HTF circulation pump is actively controlled such that a predefined target temperature is aimed at the outlet of the solar collectors. In this manner, the HTF mass flow rate is actively varied within a predefined range according to the solar irradiation conditions. In this work, the MFC is considered to operate between 40 l/m²h (reference value for HFC) and 4 l/m²h (10% thereof). This control strategy leads to three different operation regimes as shown in Fig. 3:

- **Max. flow rate regime** – In this regime, the HTF flows at its maximum flow rate (40 l/m²h). Due to the very high solar irradiation, the collector outlet temperature ($T_{coll,out}$) fluctuates above the target temperature (T_{targ}). The solar collectors are allowed to operate under this condition as long as $T_{coll,out}$ does not exceed 110 °C. If this limit is exceeded, the collector is considered to go into 'standby mode' (e.g. by means of a drain-back configuration[2] [15]). This regime is typical of summer.
- **Matched flow rate regime –** In this regime, the HTF flow rate is varied within the predefined operation range (4 – 40 l/m²h) such that $T_{coll,out}$ matches T_{targ}.
- **Min. flow rate regime –** In this regime, the HTF flows at its minimum flow rate (4 l/m²h). Due to the low solar irradiation, $T_{coll,out}$ fluctuates below T_{targ}. This regime is typical of winter.

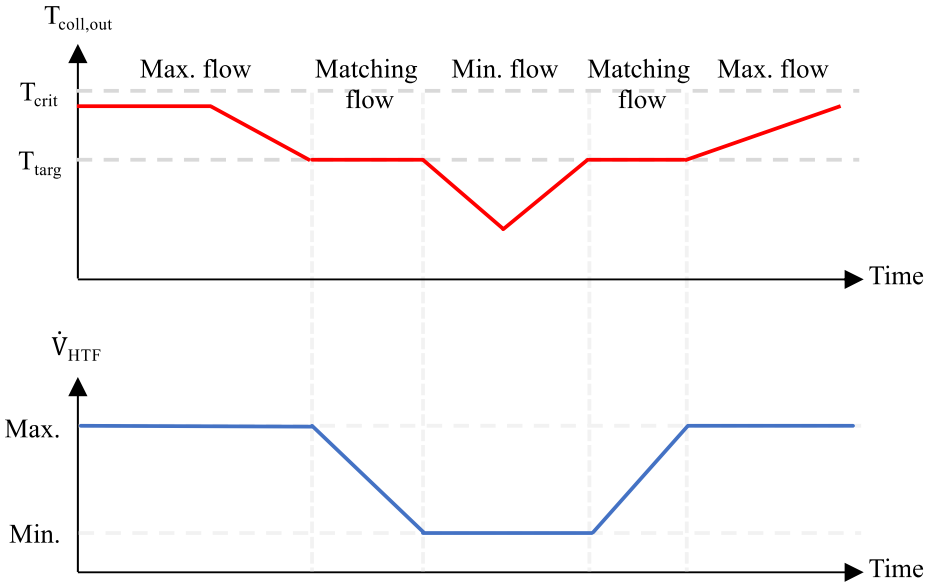

Fig. 3 – Illustration of the three different operation regimes that characterize the matched flow control

[2] A drain-back configuration prevents overheating of the heat transfer fluid by allowing the entire system to be drained at a predefined temperature below the manifold of the solar collector installation.

2.3.2 Thermal energy storage: control strategies

Heat exchangers

The energy gained by the solar collectors is transferred to the water in the STES through four heat exchangers (see Fig. 2). The HEXs are evenly distributed along the height of the storage tank and connected in series with mixing valves as shown in Fig. 4. The lowest heat exchanger (HEX 1) is located at the very bottom of the tank in order to ensure that the entire storage can be charged up to the maximum temperature. The top of the uppermost heat exchanger (HEX 4) is placed just below the bottom of the uppermost vessel (VES 3). HEX 2 and HEX 3 are evenly distributed in between HEX 1 and HEX 4.

Each HEX is equipped with a valve such that the HTF can bypass one or more HEXs depending on $T_{\text{coll,out}}$. This allows the harvested solar energy to be transferred to the storage according to the HTF temperature and maintain thereby the thermal stratification within the storage tank. The number of bypassed HEXs determine the total pressure loss in the solar circuit and consequently affect the HTF flow rate. The reference flow rates indicated in the previous section for LFC and HFC (4 and 40 l/m^{2}h) correspond to the flow rates at minimum pressure loss (e.g. HEX 2 through HTF 4 bypassed). The actual HTF flow rate is calculated at any point in time by the model based on a simplified pressure loss calculation. Table 1 shows the control strategy applied to determine which HEX are bypassed:

Vessels for DHW

The DHW is heated stepwise inside three vessels located inside the storage tank (VES 1–3), as shown in Fig. 5. Each vessel has a height of 2 m and a capacity of 300 l. The lowest vessel is fed with fresh water at a constant temperature of 10 °C – seasonal variations in the fresh water temperature are not considered. The vessels serve both the function of heat exchangers and DHW reservoirs. In designing the storage tank, the DHW temperature at the outlet of VES 3 ($T_{\text{DHW,3}} = T_{\text{DHW,out}}$) is not allowed to fall below 60 °C – this in accordance with SIA 385/1 [16]. The vessels are equally spaced along the height of the tank and connected in series by means of mixing valves. The top vessel is positioned directly below the lid of the storage tank. The arrangement of the VES can be seen in Fig. 2. The control scheme used for the provision of DHW is shown in Fig. 5. In order to achieve an exergy efficient operation, the water is mixed by means of the valves V1-V3 according to the rules shown in Table 2.

Table 1 – Control strategy used to charge the storage. $T_{\text{HEX,1}}$ through $T_{\text{HEX,4}}$ are the temperatures of the storage medium at the height at which the inlets of the HEXs are located (see Fig. 4).

Case	Conditions	Operation mode
1	$T_{\text{coll,out}} > T_{\text{HEX,4}}$ $T_{\text{HEX,4}} < 90\ °C$	HTF enters HEX 4 and flows through all HEXs. ➔ No HEX bypassed
2	$T_{\text{HEX,4}} = 90\ °C$ or $T_{\text{coll,out}} < T_{\text{HEX,4}}$ $T_{\text{coll,out}} > T_{\text{HEX,3}}$ $T_{\text{HEX,3}} < 90\ °C$	HTF enters HEX 3 and flows through HEXs 3-1. ➔ HEX 4 bypassed
3	$T_{\text{HEX,4}}, T_{\text{HEX,3}} = 90\ °C$ or $T_{\text{coll,out}} < T_{\text{HEX,4}}, T_{\text{HEX,3}}$ $T_{\text{coll,out}} > T_{\text{HEX,2}}$ $T_{\text{HEX,2}} < 90\ °C$	HTF enters HEX 2 and flows through HEXs 2-1. ➔ HEX 4 and HEX 3 bypassed
4	$T_{\text{HEX,4}}, T_{\text{HEX,3}}, T_{\text{HEX,2}} = 90\ °C$ or $T_{\text{coll,out}} < T_{\text{HEX,4}}, T_{\text{HEX,3}}, T_{\text{HEX,2}}$ $T_{\text{coll,out}} > T_{\text{HEX,1}}$ $T_{\text{HEX,1}} < 90\ °C$	HTF only flows through HEX 1. ➔ HEX 4 – HEX 2 bypassed
5	$T_{\text{HEX,4}}, T_{\text{HEX,3}}, T_{\text{HEX,2}}, T_{\text{HEX,1}} = 90\ °C$ or $T_{\text{coll,out}} < T_{\text{HEX,4}}, T_{\text{HEX,3}}, T_{\text{HEX,2}}, T_{\text{HEX,1}}$	HTF bypasses all HEXs and flows back to the solar collectors.

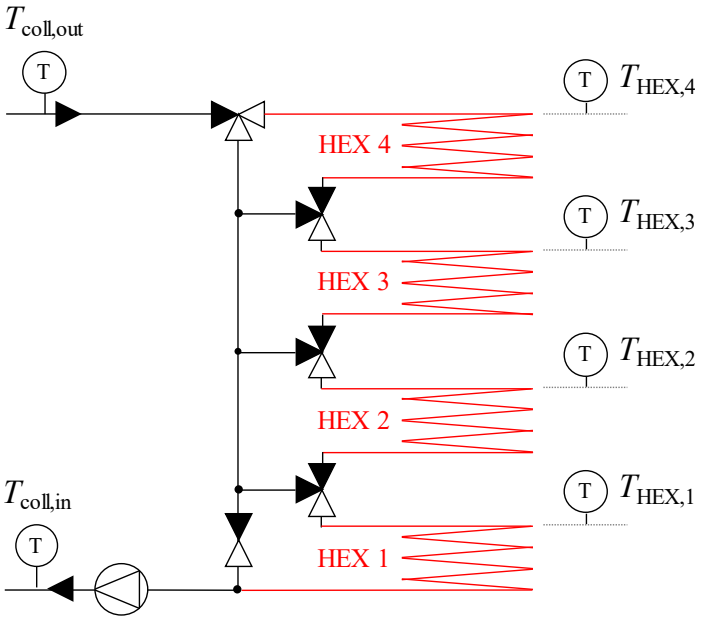

Fig. 4 – Heat exchangers (HEX) integrated inside the storage tank. Each HEX is equipped with a valve such that the HTF can bypass one or more HEXs depending on $T_{coll,out}$. $T_{HEX,1}$ through $T_{HEX,4}$ represent the temperatures of the storage medium at the height of the HEX inlets.

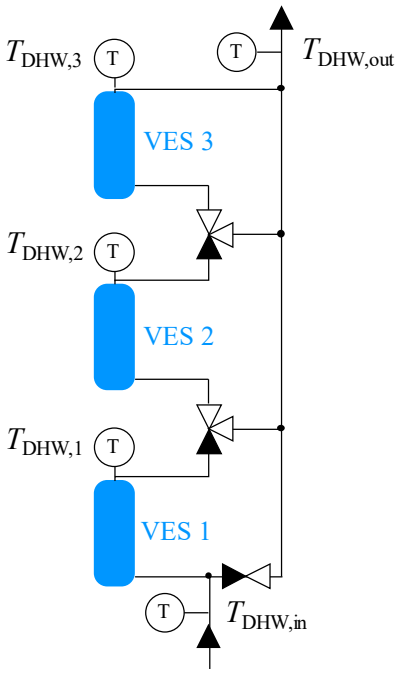

Fig. 5 – Vessels used for the production of DHW. Fresh water is supplied at a constant temperature of 10 °C. The storage tank is sized such that $T_{DHW,out}$ is 60 °C throughout the entire year.

Table 2 – Control strategy used to produce DHW at 60 °C. $T_{\mathrm{DHW},1}$ through $T_{\mathrm{DHW},3}$ are the DHW temperatures of the outlet of VES 1 through V3, respectively (see Fig. 5).

Case	Conditions	Operation mode
1	$T_{\mathrm{DHW},1} \geq 60\ °C$	Water from VES 1 and fresh water (10°C) are mixed to 60 °C.
2	$T_{\mathrm{DHW},1} < 60\ °C$ $T_{\mathrm{DHW},2} \geq 60\ °C$	Water from VES 2 and VES 1 are mixed to 60 °C.
3	$T_{\mathrm{DHW},1} < T_{\mathrm{DHW},2} < 60\ °C$ $T_{\mathrm{DHW},3} \geq 60\ °C$	Water from VES 3 and VES 2 are mixed to 60 °C.
4	$T_{\mathrm{DHW},1} < T_{\mathrm{DHW},2} < T_{\mathrm{DHW},3} < 60\ °C$	DHW cannot be supplied at the required temperature of 60 °C.

Ports

The ports allow hot water from the storage tank to be circulated in close-loop through the space heating (SH) system of the building according to the configuration shown in Fig. 6. POR 2-4 (outlet ports) are used for extracting hot water from the tank, while POR 1 (inlet port) is used for the flow returning from the SH system. $T_{\mathrm{POR},2} - T_{\mathrm{POR},4}$ represent the water temperatures at the outlet ports and T_{flow} is the flow temperature (water entering the SH system). The uppermost port (POR 4) is placed just below the bottom of the uppermost vessel (VES 3). The upper section of the tank is thereby 'reserved' solely for the production of DHW. The lowest port (POR 1) is placed at the very bottom of the tank. POR 2 and POR 3 are equally spaced between POR 1 and POR 4. The flow rate through the output ports is controlled by means of valves V2-V4, such that water is supplied to the SH system at a temperature close to 35 °C (T_{req}). The water returns to the storage via POR 1 at around 20 – 25 °C. In order to achieve an exergy efficient operation, water is extracted from the lowest possible temperature according to the rules shown in Table 3.

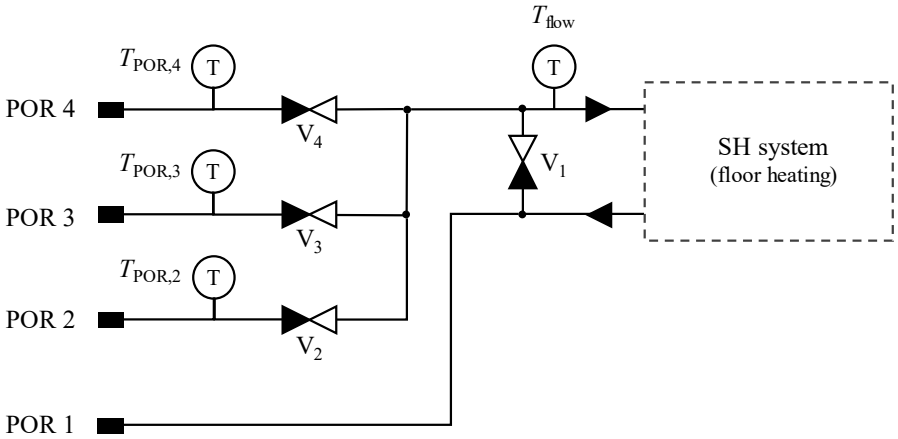

Fig. 6 – Arrangement of the ports used to circulate the hot water from the storage tank through the space heating system (floor heating) of the building

Table 3 – Control strategy used to supply hot water for the SH system at T_{req}. $T_{POR,2}$ through $T_{POR,4}$ represent the temperatures of water extracted through POR 2 through POR 4, respectively (see Fig. 6).

Case	Conditions	Operation mode
1	$T_{POR,2} \geq T_{req}$	Water is extracted from POR 2 and mixed with a fraction of the return flow.
2	$T_{POR,2} < T_{req}$ $T_{POR,3} \geq T_{req}$	Water is extracted from POR 2 and POR 3 and mixed to T_{req}.
3	$T_{POR,2}$ and $T_{POR,3} < T_{req}$ $T_{POR,4} \geq T_{req}$	Water is extracted from POR 3 and POR 4 and mixed to T_{req}.
4	$T_{POR,2} < T_{POR,3} < T_{POR,4} < T_{req}$	The heating demand of the building cannot be satisfied.

2.4 Thermal insulation materials

A comprehensive review on thermal insulation materials suitable for hot-water thermal energy storage has been carried out and published in Renewable and Sustainable Energy Reviews [17].

Paper abstract

Two different methods for insulating TES systems that are either incorporated inside residential buildings or buried underground in direct vicinity of the building are reviewed and discussed. Boundary conditions are storage volumes in the range 10 – 1,000 m^3 and storage temperatures up to 90°C. The first method (see Fig. 7) involves the application of thermal insulation materials on the outside of the storage. Thermophysical properties and costs of conventional materials (such as mineral wools and organic foams) are compared against those of state-of-the-art products such as VIP and aerogels. A parametric comparative analysis is conducted to evaluate the combined costs of thermal insulation and living space occupied by the thermal insulation for TES systems integrated inside buildings. It is shown, for example, that the use of VIP becomes advantageous when the economic value of saving living space outweighs the extra cost of VIP itself. The second method discussed is the so-called evacuated powders, in which the insulation is realized by creating an evacuated double-wall powder-containing envelope around the storage. The theoretical foundations of this method are discussed and the properties of commonly used powders – such as expanded perlite and fumed silica – are provided. Reference costs of double-wall vacuum-insulated TES tanks are provided and the use of evacuated powders is compared against the application of conventional insulation materials.

Properties and costs of selected thermal insulation materials

A selection of thermal insulation materials that can be applied on the storage outside wall is presented in Table 4 along with their most relevant thermophysical properties. The selection was made on the basis of commercially available materials with maximum service temperatures adequate for thermal energy storage in the range 60 – 90°C. Foam glass, in spite of its high thermal conductivity and high cost, has been included in this list because of its superior compressive strength – up to 1600 kPa according to EN 826 [18] – which makes it an ideal candidate for insulating the foundations of a large storage system. From the perspective of energy efficiency, the thermal conductivity is typically the most important property to be considered in the evaluation of insulating materials. The thermal conductivity, λ, largely depends on the density, internal structure (pore fraction and pore size), temperature, and moisture content of the insulation material [19–23]. For the sake of providing a concise overview, thermal conductivity values reported in the paper Table 4 correspond to dry materials at 20°C and do not include the dependence on the aforementioned variables.

The thermal performance of insulation materials can be evaluated by comparing either the thermal conductivity (λ) or the material thickness (δ) required to provide a given thermal resistance ($R = \delta/\lambda$). Here, a reference R-value of 10 m^2 K W^{-1} (suitable for seasonal TES) is used to allow a direct cost comparison of the various insulation materials. This comparison is presented in Fig. 8, in which the required material thicknesses (δ) were computed using mean thermal conductivities values of those listed in Table 4.

Conclusions (paper extract)

The use of VIP or PUR-PIR foams can be favorable when the economic value of saving living space outweighs the extra cost of the thermal insulation itself. For a storage tank of 100 m^3, for example, the use of VIP can become profitably against glass wool when the market value of real estate exceeds 1,960 €/m^2. Insulating such a tank with VIP in a dwelling in Zürich (real estate value ~9,600 €/m^2) would lead to cost savings of 110,000 € as compared to the use of conventional glass wool. As compared to VIP, PUR-PIR foams offer a more reliable solution because of the uncertainties associated to the irreversible performance degradation of VIP. To reduce this uncertainty, additional research is required to improve and demonstrate the long-term stability of VIP at temperatures suitable for TES.

While the method of evacuated powders has been used for decades in the field of cryogenics, its application at higher temperatures can offer significant advantages for TES. First, and most importantly, it can allow the storage to be buried underground, thereby eliminating the need for valuable living space inside residential buildings. Conventional insulating materials cannot offer this solution because of the intake of soil moisture that would lead to a significant increase in thermal conductivity. In contrast to VIP, the use of evacuated powders in a double-wall tank construction can allow maintaining the low thermal conductivity of the insulating jacket through a periodic re-evacuation of the vacuum chamber.

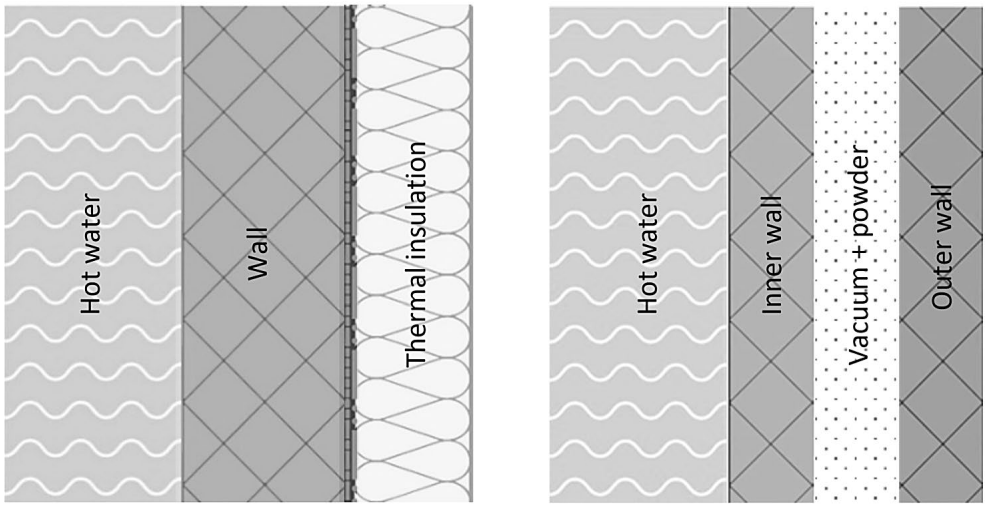

Fig. 7 – Cross-section of a thermal storage showing the arrangements considered in [17] for the incorporation of thermal insulation. Left: on the outside of the storage (e.g. using conventional thermal insulation); Right: double-wall vacuum filled with powder particles (evacuated powders).

Table 4 – Thermophysical properties of thermal insulation materials. λ: thermal conductivity at 20 °C, dry material; ρ: bulk density; T_{max}: maximum service temperature. σ_{cc} compressive stress at 10% deformation. VIP: vacuum insulation panels; XPS: extruded polystyrene; EPS: expanded polystyrene; PUR-PIR: polyurethane-polyisocyanurate foam.

Insulation material	Insulation type	λ [mW/mK]	ρ [kg/m^3]	T_{max} [°C]	σ_{cc} [kPa]	Refs.
VIP	Superinsulation	4–8	65–300	90	45–120	[24–28]
Silica aerogels	Superinsulation	4–20	3–350	750	~0–5000	[24–27,29–31]
PUR-PIR	Organic, foamy	19–30	25–100	120	100–500	[24,26,28,32–35]
XPS	Organic, foamy	25–35	20–80	75	150–700	[26,28,33,34,36]
EPS	Organic, foamy	29–41	10–50	80	60–260	[26,28,33,34,36,37]
Glass wool	Inorganic, fibrous	30–46	8–150	500	15–80	[22,24,26,28,33,34]
Rock wool	Inorganic, fibrous	33–46	13–240	750	15–80	[22,28,33,38]
Foam glass	Inorganic, foamy	38–61	100–200	>400	400–1600	[26,39–43]

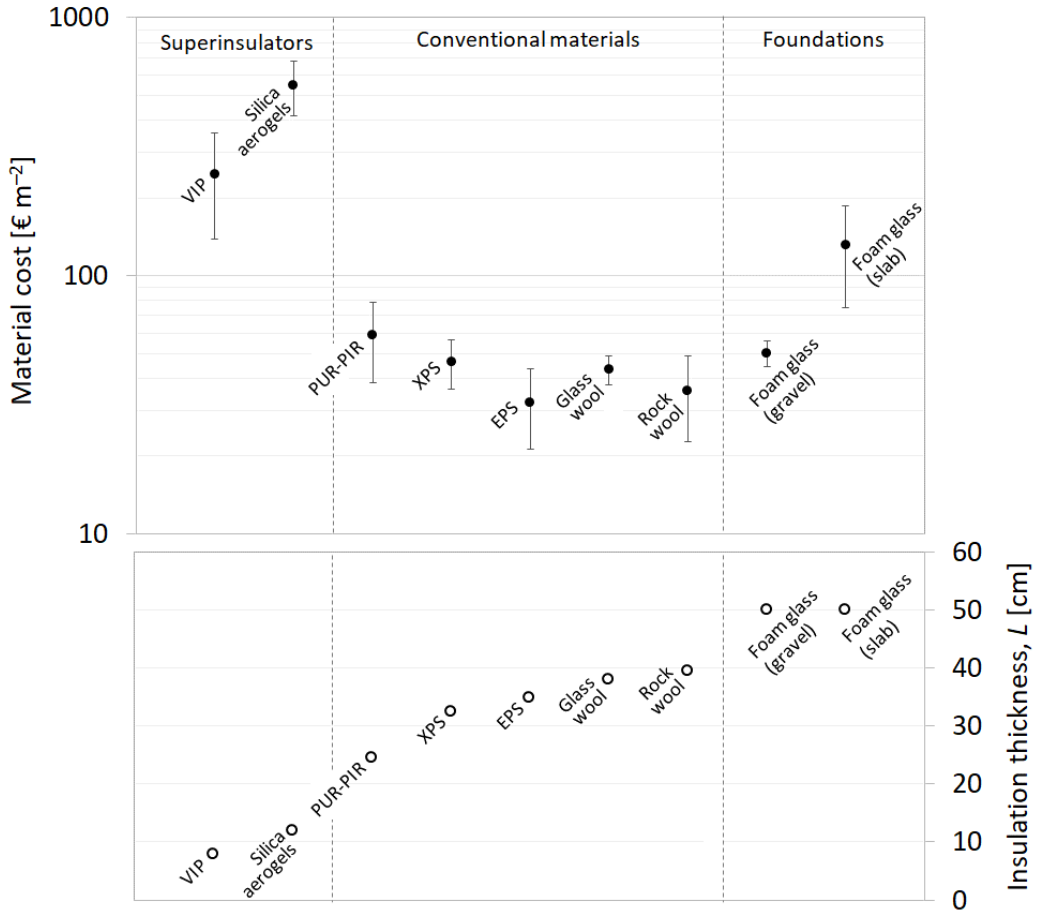

Fig. 8 – Material cost (top) and insulation thickness (bottom) required to achieve an R-value of 10 m^{2}K/W with various thermal insulation materials. Solid dots represent average cost values, while the bars indicate the range found in the literature.

3 Numerical models

The applied system model consists of three 'sub-models': (1) thermal energy storage model, (2) solar collector model, and (3) building model. A system of differential equations is used to describe the complex dynamics of each components and their close interaction. An ordinary differential equation using a set of time-dependent component variables (e.g. the room temperature in the building) models the solar collector and the building. The solution of the energy conservation equation models the thermal energy storage and its internal sub-components. The sub-models are linked to each other for data transfer.

The solar collector and the building model were adapted from the EU project Heat4Cool [44,45]. The in-house thermal energy storage model has been developed in the framework of the SCCER HaE research activities related to the task "Sensible Seasonal Thermal Energy Storage" led by HSLU.

The overall structure of the system model is shown in Fig. 9. The model has both an inner and outer time loop. The inner time loop solves the energy equations with different time-steps. The time step for the storage model is 10 s, while the solar collector and the building model use a variable time step up to 180 s, defined by the model solving algorithm itself. The outer time loop defines the transfer of the calculated data. These data establish the boundary conditions of each sub-model for 180-second intervals.

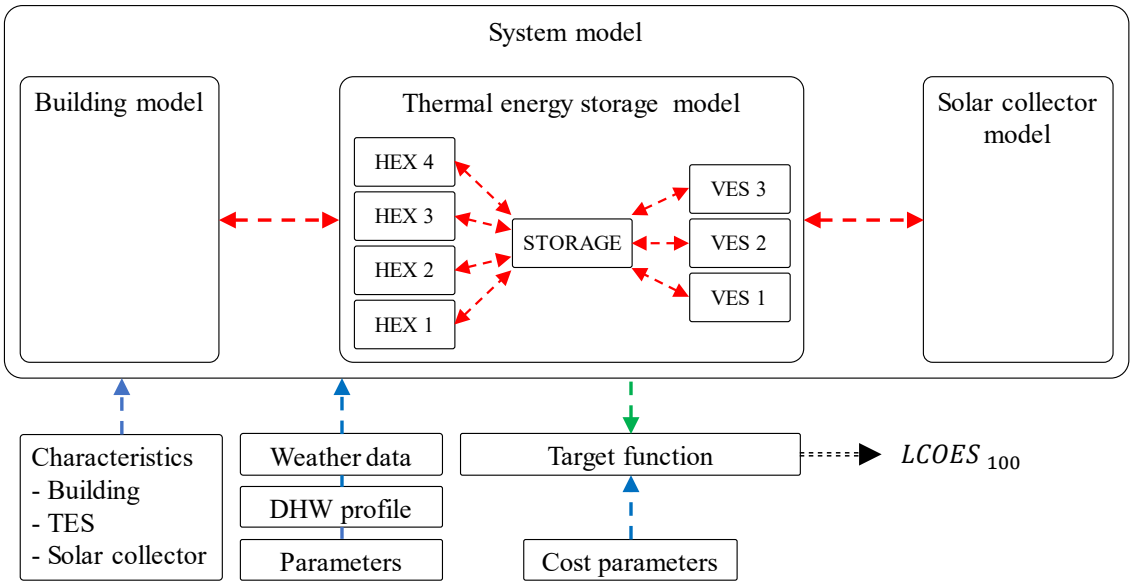

Fig. 9 – Schematic representation of the model architecture. Blue arrows: input data; red arrows: exchange of data during execution; green arrows: raw data output stream.

3.1 Mathematical model descriptions

Solar collectors

The heat generated by a solar thermal panel $\dot{Q}_{\text{coll}}$ is calculated with the following equation:

$$\dot{Q}_{\text{coll}} = \eta_0\, I(t) A_{\text{coll}} - C_1(T_{\text{coll}} - T_{\text{amb}})A_{\text{coll}} - C_2(T_{\text{coll}} - T_{\text{amb}})^2 A_{\text{coll}} \tag{3-1}$$

Where $I(t)$ is the solar irradiation at the considered location with the given panel orientation and inclination, T_{coll} and T_{amb} are the collector and ambient temperature, respectively, and A_{coll} is the collector area. The parameters C_1, C_2 and the efficiency η_0 are collector-dependent parameters. The collector temperature is determined as follow:

$$T_{\text{coll}} = 0.5(T_{\text{in}} + T_{\text{out}}) \tag{3-2}$$

Where T_{in} and T_{out} are the temperature of the HTF entering and exiting the solar collector.

Thermal energy storage

The thermal energy storage model consists of eight energy conservation equations. One equation describes the temperature distribution of the hot-water storage, while the remaining seven equations describe the internal sub-components (4 HEXs and 3 VESs). Source terms interlink HEX and VES equations with the storage equation. The following assumptions are made:

- Radial temperature gradients are neglected
- No phase change occurs
- All flows are fully developed

The following conservation equation expresses the temperature distribution of the storage:

$$\begin{aligned}\rho_w c_{p,\text{w}} \frac{\partial T_w}{\partial t} = \lambda_w \frac{\partial^2 T_w}{\partial z^2} - \rho_w c_{p,\text{w}} u \frac{\partial T_w}{\partial z} + \sum_i U_{i,HEX}\, A_{i,HEX}\left(T_w - T_{i,HEX}\right) \\ + \sum_j U_{j,\text{VES}}\, A_{j,\text{VES}}\left(T_w - T_{j,\text{VES}}\right) + \sum_k \frac{\dot{m}_k c_{p,\text{w}}}{V_k}\left(T_w - T_{k,POR}\right) \\ + U_{loss} A_{loss}(T_w - T_{\text{room}})\end{aligned} \tag{3-3}$$

Where ρ is the density, c_p the specific heat capacity, λ the heat transfer coefficient, T the temperature, z the direction (starting at the bottom of the storage tank) and u is water velocity inside the storage. U represents the overall heat transfer coefficient, A the heat transfer area, V the volume and $\dot{m}$ the mass flow rate entering the storage tank. The source terms represent:

- Energy exchange between the HTF in the HEXs and the storage medium in the tank
- Energy exchange between the DHW in the vessels and the storage medium in the tank
- Energy extraction/insertion of water through the ports for space heating
- Energy losses over the tank outer surface

Convection effects within the storage are neglected. In scenario 1, convection on the outside lateral surfaces is modelled by considering the air gap between the storage tank and the surrounding shaft. In scenario 2, only convection at the top surface of the tank is considered (all other surfaces are in direct contact with the surrounding soil).

A node-mixing model determines the effects of buoyancy-induced mixing. Increases in fluid density at lower temperatures cause cooler layers to sink and warmer layers to rise. The node-mixing model considers a point in time when a warmer layer $i+1$, positioned below a cooler layer i, completely mixes reaching a uniform temperature. This is expressed by:

$$T_{i+1}^{new} = T_i^{new} = \frac{m_i c_{p,i} T_i + m_{i+1} c_{p,i+1} T_{i+1}}{m_i c_{p,i} + m_{i+1} c_{p,i+1}} \tag{3-4}$$

Heat exchangers

The temperature distribution in the heat exchangers is determined by:

$$\begin{aligned} \rho_{\mathrm{HTF}} c_{\mathrm{p,HTF}} \frac{\partial T_{\mathrm{i,HTF}}}{\partial t} &= -\rho_{\mathrm{HTF}} c_{\mathrm{p,HTF}} u \frac{\partial T_{\mathrm{i,HTF}}}{\partial z} + U_{\mathrm{i,HEX}} A_{\mathrm{i,HEX}} \left(T_{\mathrm{i,HTF}} - T_{\mathrm{w,STO}}\right) \\ &+ \frac{\dot{m}_{\mathrm{in}} c_{\mathrm{p,HTF}}}{V} T_{\mathrm{in,HTF}} + \frac{\dot{m}_{\mathrm{out}} c_{\mathrm{p,HTF}}}{V} T_{\mathrm{out,HTF}} \end{aligned} \tag{3-5}$$

Where the sub-index i stands for one of the four HEX. Conduction within the HEX is neglected as the convective heat transfer is assumed to dominate. The source terms represent:

- Energy exchange between the HTF in the HEX and the storage medium in the tank
- Energy exchange by means of extraction/insertion of HTF from/to the HEX

The following formula describes the heat transfer coefficient between the HTF and the water in the tank:

$$U_{\mathrm{HEX}} A_{\mathrm{HEX}} = \frac{1}{\frac{1}{h_i} + \sum \frac{r_i}{\lambda_{\mathrm{steel}}} \ln\left(\frac{r_o}{r_i}\right) + \frac{r_i}{r_o} \frac{1}{h_o}} \tag{3-6}$$

Where r stands for the radius. The convection heat transfer coefficient h_i and h_o are calculated according to [46].

Vessels for DHW

The temperature distribution in the vessels is determined by:

$$\begin{aligned} \rho_{\mathrm{w}} c_{\mathrm{p,w}} \frac{\partial T_{\mathrm{i,w,VES}}}{\partial t} &= -\rho_{\mathrm{w}} c_{\mathrm{p,w}} u \frac{\partial T_{\mathrm{i,w,VES}}}{\partial z} + U_{\mathrm{i,VES}} A_{\mathrm{i,VES}} \left(T_{\mathrm{i,w,VES}} - T_{\mathrm{w,STO}}\right) \\ &+ \frac{\dot{m}_{\mathrm{in}} c_{\mathrm{p,w}}}{V} T_{in,\mathrm{w},VES} + \frac{\dot{m}_{\mathrm{out}} c_{\mathrm{p,w}}}{V} T_{\mathrm{out,w,VES}} \end{aligned} \tag{3-7}$$

Conduction heat transfer within the vessel is neglected as the convective heat transfer is assumed to dominate. The heat transfer coefficient between the water in the vessels and the water in the tank is described by:

$$U_{\mathrm{VES}} A_{\mathrm{VES}} = \frac{1}{\frac{1}{h_i} + \frac{r_i}{\lambda_{\mathrm{steel}}} \ln\left(\frac{r_o}{r_i}\right)} \tag{3-8}$$

The inner convection h_i was calculated according to [47]. External convection was neglected due to the weak mass flow rate in the tank.

Solution method

The discretized equations use the finite volume method with uniform spacing. Spatial discretization of the diffusion terms and convection terms employ a central differencing scheme and up-/downwind scheme respectively. Time discretization utilizes the fully implicit, backward directed differentiation scheme which guarantees unconditional time-step stability.

The thermo-physical properties of water were fitted to algebraic functions of temperature. The thermophysical properties of the water-glycol mixture are treated as temperature independent. The latter are taken from [48].

Building model

The building dynamics are modelled by a single room temperature T_{room}, which is described by the following energy conservation equation:

$$C\dot{T}_{\text{room}} = gI(t) + \dot{Q}_{\text{heat}} + \dot{Q}_{\text{TES}} - H(T_{\text{room}} - T_{\text{amb}}) \tag{3-9}$$

The change of the room temperature is caused by the solar gain $gI(t)$, the heat flux of the emitter system $\dot{Q}_{\text{heat}}$, the heat contributions from the heat loss of the thermal energy storage $\dot{Q}_{TES}$, and the losses through the building surfaces $H(T_{\text{room}} - T_{\text{amb}})$. The parameters C, g, and H are determined based on the properties of the building (defined by the user) as follows.

Heat loss factor (H)

The heat loss factor of the building includes a transmission part and a convection part. The transmission part includes the heat loss through areas of the building envelope characterized by their U-values and an allowance for thermal bridges using a coefficient expressed as an increment to the U-values. The convection part includes the heat exchange by (intended) ventilation and/or (unintended) air leakage.

$$\begin{aligned} H = {} & U_{\text{walls}}A_{\text{walls}} + U_{\text{roof}}A_{\text{roof}} + U_{\text{floor}}A_{\text{floor}} + U_{\text{windows}}A_{\text{windows}} \\ & + \Delta U_{\text{thermal bridges}}(A_{\text{walls}} + A_{\text{roof}} + A_{\text{floor}} + A_{\text{windows}}) \\ & + (N_{\text{ventilation}} + N_{\text{air leakage}})V\rho_{\text{air}}c_{\text{air}} \end{aligned} \tag{3-10}$$

The U-values are user defined input values. The impact of thermal bridges considered here are based on a simplified coefficient $\Delta U_{\text{thermal bridges}}$ that captures the average impact of all thermal bridges in the building. The ventilation behavior $\left(N_{\text{ventilation}} + N_{\text{air leakage}}\right)$ of the buildings is modelled according to [49].

Thermal capacity (C)

The effective thermal capacity of both external and internal walls and slabs estimates the thermal capacity of the building using a simplified equation.

$$C = c_{\text{walls}}A_{\text{walls}} + c_{\text{int}}A_{\text{int}} \tag{3-11}$$

As the area of the internal walls is not known, a simplified approximation is employed where the area of the internal walls is twice the area of the external walls. The latter is calculated based on the user's input.

Solar gain factor (g)

The solar gain factor represents the effective area of the building for the collection of solar irradiance. Four different factors for each orientation are calculated:

$$g_{\text{direction}} = g_{\text{windows}} A_{\text{windows,direction}} F_{\text{frame}} \tag{3-12}$$

Where direction is either south, east, west, or north. g_{windows} is the solar conversion factor of the window, $A_{\text{windows,X}}$ is the area of the windows in direction X given a perfect north-south orientation of the building and F_{frame} is the so-called frame factor. The areas of the windows for the respective sides are calculated based on the user's input. To calculate the total solar contribution

$$g \cdot I(t) = g_{\text{south}} I_{\text{south}}(t) + g_{\text{east}} I_{\text{east}}(t) + g_{\text{west}} I_{\text{west}}(t) + g_{\text{north}} I_{\text{north}}(t) \tag{3-13}$$

The contribution of direct and diffuse radiation for all four directions is calculated based on the sun's current position employing the Perez Sky model [50] and a multi-linear transfer function for the diffuse radiation through the windows [51]. The solar conversion factor is estimated based on the *U*-value of the windows according to the following approximation formula [44,45]:

$$g_{\text{windows}} = (0.125\, U_{\text{windows}})^{0.25} \tag{3-14}$$

4 Storage model validation

The thermal energy storage model has been validated using own experimental data collected at HSLU (storage without internal HEX) and data from the literature (storage with internal helical HEX).

4.1 Validation with HSLU data

Experimental data for validation purposes was acquired at HSLU using a hot-water tank setup with the following characteristics:

- Storage volume: 1.3 m^3 (diameter: 0.98 m, height: 2 m)
- Pressure: Unpressurized (atmospheric pressure)
- Thermal insulation: None
- Wall material: Plexiglass (1 cm thick)
- Bottom and lid: Steel (2 mm thick)

Three ports located at different tank heights served as inlets. Each port allowed an independent adjustment of the flow rate during operation. In addition to the three inlets, the outlet port was located at the very bottom of the storage tank.

Two lances, each with 10 temperature sensors, were used to measure the temperature distribution within the storage tank. The sensors were PT100 class A with an accuracy of ± 0.15 °C. One lance was placed in the middle of the storage tank while the second was placed at a distance of 2 cm apart from the lateral wall. The location of the second lance was selected to avoid measuring temperatures where buoyancy occurs. Each lance had evenly distributed sensors along the height of the tank with a distance of 10 cm to each other. With the two lances, two sensors were installed at each height and the mean value at each height was used for the validation. In addition, two temperature sensors were installed in the pipes with immersion pockets close to the ports to determine the input and output temperatures. The mass flow rate going into the storage was measured with a Coriolis Promass F300 flow meter with an accuracy of ± 0.05% [52].

A series of seven experiments were carried out for different charging/discharging profiles. The initial temperature of the water in the storage tank was about 20 °C. Hot water was pumped into the thermal storage tank via one of the three ports with a constant mass flow rate. The hot water rises due to the difference in density between the hot and cold water. Once the upper part of the tank was thermally charged, hot water displaced cold water below until the entire tank was fully charged with hot water. Water at the same mass flow rate exists through the outlet port at the bottom of the tank. Temperatures and mass flow rates were recorded at an interval of 10 s. The duration of an experimental run was approximately 5 h.

Experiments were performed with two different Reynolds numbers: 5'000 and 10'000. Fig. 10 shows the temperature evolution within the tank for the experimental run with $Re = 10'000$. The lowest port was used as inlet. The x-marks represent the measured data points and the solid lines the simulated temperatures. The results above the inlet port correlate well.

4.2 Validation with literature data

An additional model validation was performed by comparing the simulation results to a validated model from literature [46]. The validation model accounts for heat transfer effected by heat exchangers placed inside a storage tank, the effects of buoyancy-induced mixing, and thermal stratification within the storage. The validation model considers a cylindrical hot-water tank and a helix HEX with the specifications listed below:

- Storage volume: 2.5 m^3 (diameter: 1.25 m, height: 2 m)
- HEX material: Stainless steel
- Coil pitch / diameter: 36.2 mm / 0.49 m
- Inner tube diameter: 21.6 mm
- Outer tube diameter: 26.9 mm
- Length of coil: 85.1 m

Fig. 11 shows a comparison and the good agreement obtained between the temperature profiles computed by our model (solid lines) with those reported in the literature (crosses). The plotted profiles correspond to the water temperature at a height of 0.1 and 1.9 m.

4.3 Energy balance

An energy balance is performed for each simulation to verify the integrity of the computed results. All energy flows into and out of the thermal energy storage are considered. To calculate the energy content of the VES and HEX it is assumed that the volumes occupied by the HEX and VES within the tank have the same temperatures as the corresponding layers in the tank in which they are located. The energy content of the materials comprising the HEX and VES themselves are neglected. The error in the energy balance is thus computed at every time step as:

$$E_{\text{error}} = E_{\text{solar}} - \sum_i E_{VES,i} - E_{\text{losses}} - \frac{dE_{\text{TES}}}{dt} \tag{4-1}$$

The errors in this simulation campaign ranged from 0.2 to 0.6%.

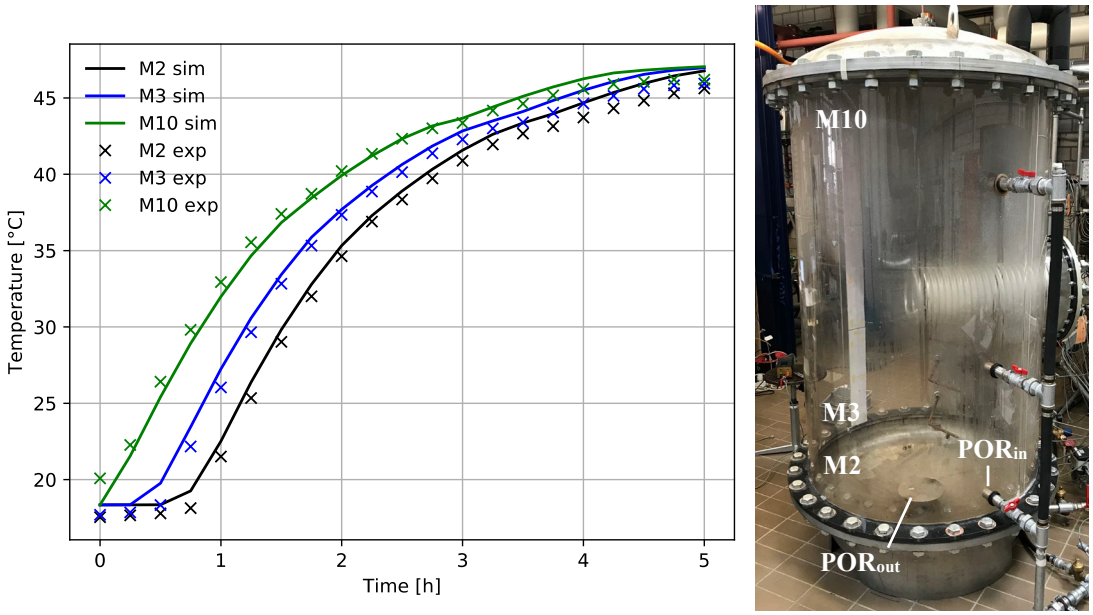

Fig. 10 – Left: Comparison of simulation results with experimental data acquired with HSLU's hot-water tank setup. Right: HSLU's hot-water experimental setup showing the locations of the temperature measurements and the inlet and outlet ports.

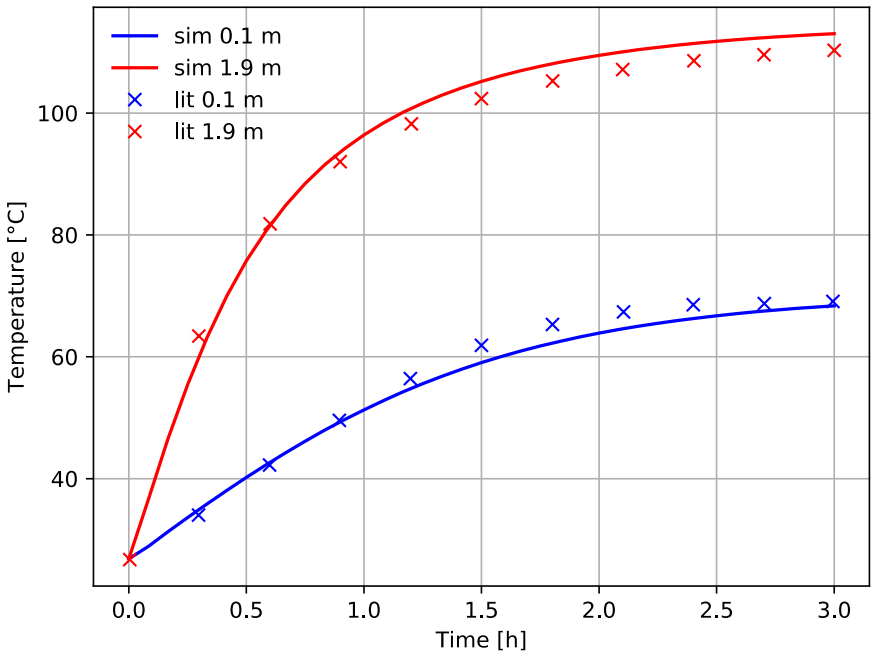

Fig. 11 – Comparison of simulation results obtained with the model of this project with simulation results of the experimentally validated model presented in [46].

5 Methodology

5.1 Boundary conditions

The storage is considered to operate at atmospheric pressure and its temperature is consequently limited to 90 °C. The temperature of the DHW at the outlet of the uppermost vessel needs to be at least 60 °C according to SIA 385/1 [16].The room temperature inside the building is regulated to 20 °C. Additional boundary conditions include the characteristics of the reference building and the weather data – these are described below.

5.1.1 Reference building

The size of the multifamily house and the number of inhabitants have a direct impact on the space heating and DHW requirements of the building. A detailed analysis of the Swiss building stock was carried out based on data of the Swiss Federal Statistical Office [53] and the building regulations of the cantons Bern and Zürich [54,55] to define a representative reference building model for this project.

Building age

The target of this project are existing Swiss multifamily houses. Given that the integration of STES in existing buildings can be expected to require significant renovation measures, only buildings built in the period 1961-1990 were considered. Newer buildings might not require yet a renovation or at least not to an extent that would justify the investment costs associated to the integration of a STES system.

Number of apartments and floors

Statistically, most of the multifamily houses built during the aforementioned construction period have 6 – 9 apartments, and 3 – 5 floors [56]. Based on this, a reference building with 8 apartments distributed over 4 floors (two per floor) was chosen for this study.

Number of rooms, floor space and floor area

Half of the Swiss population lives in apartments with 3 – 4 rooms [57]. In the construction period considered, the number of 3-room apartments is significantly higher than that of 4-room apartments. However, given that the total living space of the 4-room apartments is about 20% larger and offers thus a larger impact, the reference object taken for this analysis consists of 4-room apartments. The living area per apartment is taken here at 100 m^2. This corresponds to the statistical mean value of living space associated to 4-room apartments in the construction period considered.

The total energy reference area of the building has been estimated at 924 m^2. This includes the living area of two apartments and the area taken up by the inner and outer walls and the staircase. The area occupied by the staircase was estimated according to the minimum requirements for emergency escape routes defined in the Swiss fire protection guidelines [58].

Window area

The total window area was determined on the basis of building regulations of various cantons. Due to the different ordinances, the smallest size was chosen. This amounts to 10% of the living space of the apartment. The percentage distribution of the windows on the different house sides were takes as follows: south 55%, north 25% and east/west 10%.

Roof area

The available roof area (374 m^2) was calculated based on a roof with an inclination angle of 45° and no overhang. The orientation of the house is such, that one roof is facing north, the other one south. As a result, the solar collector area is limited to a maximum of 187 m^2 (roof area facing south). The parametric study presented in Section 5.4 involves variation of the tilt angle of the solar collectors (and thus indirectly the roof inclination angle) to assess the potential of reducing the costs by means of optimizing this parameter.

Occupancy density

In Switzerland, an average of 2.5 persons live in a 4-room apartment. In order to match this occupancy density, the reference house was assumed to be occupied by a total of 20 inhabitants.

Heating energy demand

The house is heated to set temperature of 20 °C during the heating period. Floor heating is assumed to be the emitter system in the building. The heating was designed at a temperature of −10 °C whereby the flow temperature of the heating is assumed to be approx. 35 °C. Given these conditions, the heating system is required to provide a thermal output of around 10 kW to heat the reference building.

Domestic hot water profile

Each person consumes in Switzerland on average about 50 l of hot water at 60 °C per day [59]. To generate a realistic DHW profile of the multifamily house, the tool DHWcalc (version 2.02b) of the University of Kassel was used [60]. The program distributes DHW draw-offs throughout the year with statistical means, according to a probability function. Both the boundary conditions for the tap events (volume flows, tap durations, etc.) and for the probability function (daily, weekly, seasonal distribution of the tap events, etc.) is chosen as representative as possible for Switzerland.

5.1.2 Location and weather

The location of the reference building determines the weather conditions (solar irradiation and outside temperature) to be used in the dynamic thermal simulations. In Switzerland, there is no single geographical location that can be deemed ‘representative’ of the Swiss weather. Hence, two different locations have been considered in this study: Zurich and Bern. These cities were chosen as the reference as they exhibit the highest density of buildings with 6 – 9 apartments as shown in Fig. 12 [56]. These locations have well documented weather data available from MeteoSchweiz [61] and are thus suitable for the numerical study conducted in this work.

The weather parameters required for the model are: air temperature, diffuse and direct radiation. The weather data used in the simulations were obtained from Meteonorm [62]. For both locations, the climate values of Meteonorm 7 were used, whereby the temperature parameters period considers the years 2000 – 2009 and the radiation parameters period the years 1991 – 2010. The data are resolved hourly as mean values.

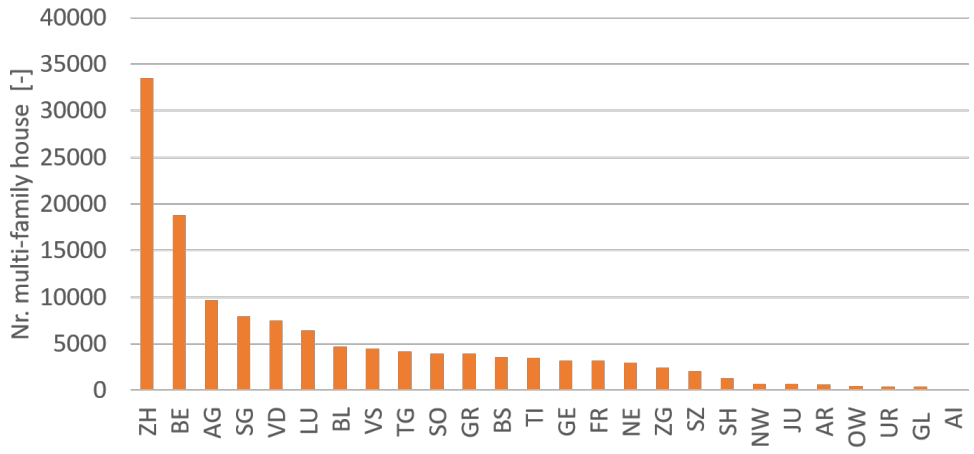

Fig. 12 – Number of buildings with 6 – 9 apartments for each of the Swiss Cantons

5.1.3 Solar model

For the simulation, the Variosol E antireflex solar collectors from Winkler Solar GmbH were used. The collector efficiency η_0 and the constants C_1 and C_2 were taken from the manufacturer data sheet [63]. The properties of the glycol required for the simulation were taken at 70 °C.

5.2 Target function

The optimization parametric study (see Section 5.4) will serve to identify the most cost-effective storage configurations based on different thermal insulation concepts and control strategies. In this project, the cost of the system is described by LCOES_{100}: the Levelized Cost of Energy Storage with a self-sufficiency grade of 100%. LCOES_{100} describes the cost per kWh of energy output of the storage, whereas $k_{VK,AF}$ is the annual full cost and W the annual energy output of the storage:

$$\mathrm{LCOES}_{100} = \frac{k_{VK,AF}}{W} = \frac{\mathrm{CAPEX} \cdot \mathrm{ANF} + \mathrm{OPEX}}{W} \tag{5-1}$$

Note that LCOES_{100} is calculated based on the actual energy output of the storage and not the nominal storage capacity. Given that the building has a self-sufficiency grade of 100%, the energy output W equals the total annual heat demand. Capital expenditure (CAPEX) is calculated as the sum of costs of the building internal reconstruction (K_{const}, which only applies when the storage is incorporated inside an existing building), components (K_{com}), installation (K_{inst}), and living space lost ($K_{\mathrm{imo,loss}}$):

$$\mathrm{CAPEX} = K_{\mathrm{const}} + K_{\mathrm{com}} + K_{\mathrm{inst}} + K_{\mathrm{imo,loss}} \tag{5-2}$$

The cost of the system components (K_{com}) are those of the solar collectors and the storage tank (including its internal components such as HEX and VES). The costs for installation comprise the installation of the storage (in the building or underground) and the solar collector system. The component costs are given by the sum of the costs of the tank itself (K_{tank}), vessels K_{VES}, heat exchangers K_{HEX}, thermal insulation (K_{ins}), and solar collectors K_{sol}:

$$K_{\mathrm{com}} = \underbrace{K_{\mathrm{tank}} + N_{\mathrm{VES}} \cdot K_{\mathrm{VES}} + N_{\mathrm{HEX}} \cdot K_{\mathrm{HEX}} + K_{\mathrm{ins}}}_{\text{Cost of thermal storage incl. thermal insulation and internal components}} + K_{\mathrm{sol}} \tag{5-3}$$

Where N_{VES} and N_{HEX} represent the number of VES and HEX, respectively. The installation costs K_{inst} are split in two terms: the cost for installing the solar collectors ($K_{\mathrm{inst,sol}}$) and those for installing the storage itself ($K_{\mathrm{inst,TES}}$):

$$K_{\mathrm{inst}} = K_{\mathrm{inst,sol}} + K_{\mathrm{inst,TES}} \tag{5-4}$$

The operational expenditures (OPEX) are calculated with an operational factor β and the investment costs of the STES system:

$$\mathrm{OPEX} = \beta\left(\mathrm{CAPEX} - K_{\mathrm{imo,loss}} - K_{\mathrm{const}}\right) = \beta\left(K_{\mathrm{com}} + K_{\mathrm{inst}}\right) \tag{5-5}$$

The annuity factor (ANF) is given by the following formula with interest rate i and payback period n:

$$\mathrm{ANF} = \frac{(1+i)^n \cdot i}{(1+i)^n - 1} \tag{5-6}$$

Table 5 provides an overview of the values used for the cost calculations. The values were determined by means of a combined industry survey and an extensive literature review.

5.2.1 Terms of the target function

The following terms are calculated differently depending on the scenario under consideration.

- K_{const} – In scenario 1, the storage is placed inside the building and extends over several floors. In this case, the costs are calculated as a function of the number of floors (N_{floors}), the cross-sectional area of the storage (A_{TES}, which includes the thermal insulation), and the reconstruction costs ($k_{\text{imo\_min}}$). Here, $N_{\text{floors}} = 4$ as the area lost in the basement of the building is not accounted for in the cost calculations.

$$K_{\text{const,1}} = N_{\text{floors}} \cdot A_{\text{TES}} \cdot k_{\text{imo\_min}} \tag{5-7}$$

  In scenario 2, where the storage is buried underground in direct vicinity of the building, the excavation costs are calculated as a function of the total storage volume including the thermal insulation (V_{TES}). The excavation costs, especially when the hole is narrow, increases dramatically with the depth of the hole.

$$K_{\text{const,2}} = V_{\text{TES}} \cdot k_{\text{exc}} \tag{5-8}$$

- $K_{\text{imo,loss}}$ – In scenario 2, there is no loss of living room and therefore this term becomes zero. In scenario 1, a distinction is made between the three cases:
  - Retrofit (RF): Direct loss of existing living space.
  - New building, footprint affected (NB-FA): Loss of potential living space (opportunity costs). The opportunity costs are given by the real state value minus the construction costs that would have to be incurred. The constructions costs are taken at 3'800 CHF/m^2.
  - New building, footprint unaffected (NB-FU)**:** No loss of existing or potential living space.

- β – The operational factor is different for the two scenarios considered. In scenario 2, β is considered higher because of the lower technology readiness level (TRL) and increased complexity of the vacuum insulated tank technology.

- K_{ins} – In scenario 1, the costs vary depending on the insulation material used. In scenario 2, the cost of the thermal insulation is zero given that the insulation is incorporated in the wall of the tank itself.

Table 5 – Values of the various costs parameters. Sources: industry survey and literature review.

K_{VES}			20 CHF/l
K_{HEX}			$150 \cdot A_{HEX} + 140$ CHF
$K_{imo,loss}$	Scenario 1 Case: RF	Bern: Zurich:	6'000 CHF/m^2 12'000 CHF/m^2
	Scenario 1 Case: NB-FA	Bern: Zurich:	2'200 CHF/m^2 8'200 CHF/m^2
K_{ins}		GW: PIR/PUR: VIP: XPS:	110 CHF/m^3 360 CHF/m^3 4'000 CHF/m^3 180 CHF/m^3
$K_{inst,TES}$			$62 \cdot V_{tank} + 9000$ CHF
$K_{inst,ins}$			100 CHF/m^2
$K_{inst,sol}$			$260 \cdot A_{sol} + 9000$ CHF
K_{sol}			$300 \cdot A_{sol} + 200$ CHF
K_{tank}		Scenario 1: Scenario 2:	$470 \cdot V_{TES} + 1900$ CHF $6900 \cdot V_{TES}^{0.504}$ CHF
k_{exc}			$60 \cdot H_{tank} + 100$ CHF/m^3
k_{imo_min}			2'200 CHF/m^2
i			1%
n			20 years
β		Scenario 1: Scenario 2:	0.005 (0.5%) 0.02 (2.0%)

5.3 Optimization parameters

The aim of the parametric-based optimization study was to identify the most cost-effective storage configurations and the potential for the reduction of $LCOES_{100}$. The aspects to be optimized include the solar collector control strategy to charge the tank and the thermal insulation (material and thickness) to be used. The selected parameters are described below. The schematic representation of the methodology used to conduct the parametric study is shown in Fig. 13 (scenario 1) and Fig. 14 (scenario 2).

Parameters used in both scenarios

- α_{coll}: Tilt angle of the solar collectors. A low angle increases the solar yield in summer, while a high angle increases the production in winter. The parametric study presented in Section 5.4 involves variation of the tilt angle of the solar collectors (and thus indirectly the roof inclination angle) to assess the potential of reducing the costs by means of optimizing this parameter.
- A_{coll}: Net area of the solar collector installation. A larger solar collector area leads to an increased solar yield and thus to a smaller storage volume required. In the analysis, the maximum collector area is limited by the available roof area of the building.

- Control strategy of the solar collectors (HFC, LFC, or MFC). The control strategy is defined by: (1) whether the flow rate of HTF is actively controlled or not, (2) the value or range of the flow rate, and (3) the solar collector target temperature (T_{targ}).

Parameters varied only in scenario 1

- Insulation material (λ_{ins} and K_{ins}). The insulation material has an influence on the insulation thickness required to achieve a given thermal resistance (R-value), which in turn has an influence on the total volume occupied by the storage and ultimately on the extent of living space lost. Glass wool is the most common thermal insulation material used and is thus taken for the baseline case.
- R-value: To allow a direct comparison between the different insulation materials, the R-value – instead of the insulation thickness – is used in this work. The R-value is defined as $R = \delta/\lambda$. Where δ is the thickness of the thermal insulation A baseline R-value of 7.4 m^2K/W is used for the parametric study – this corresponds to glass wool at 60°C and a thickness of 30 cm.

Parameters varied only in scenario 2

- h_{TES} (tank height): Because the thermal insulation of the double-wall vacuum insulated tank cannot be changed (integral part of the tank), the height of it has been varied instead as part of the parametric study. This has a direct influence on CAPEX and therefore on LCOES_{100}, since the excavation cost increase dramatically with the height of the storage.

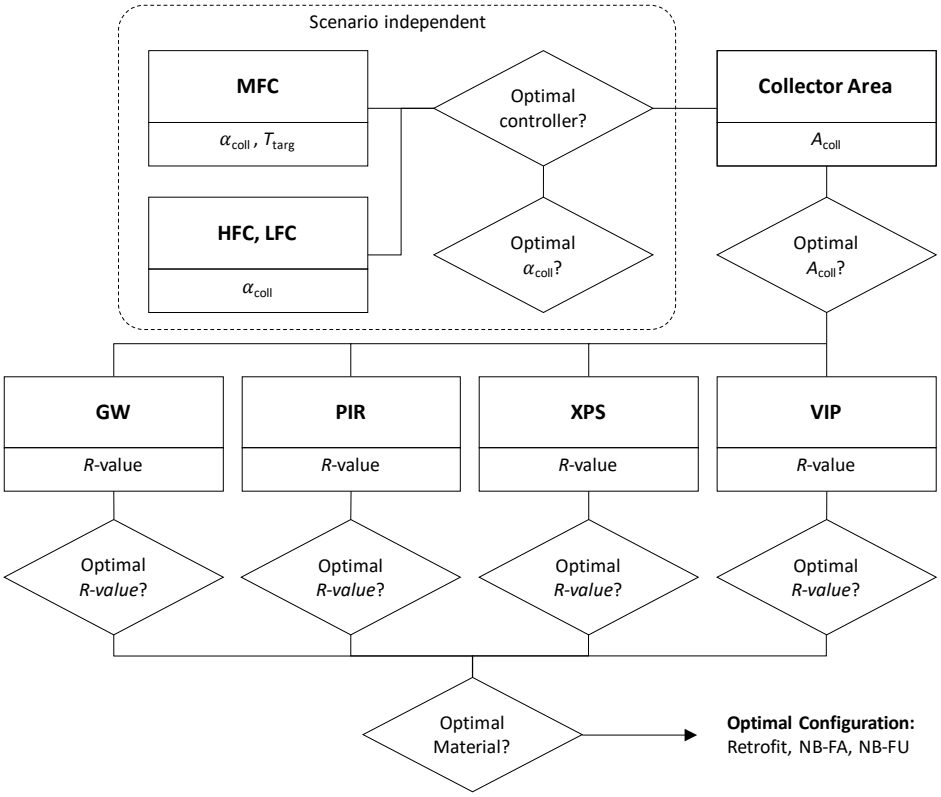

Fig. 13 – Methodology applied for the parametric study for scenario1 (storage inside the building)

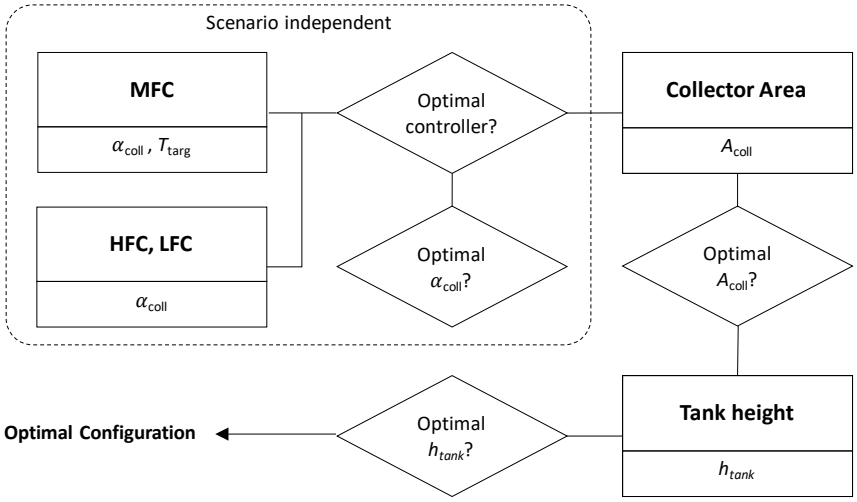

Fig. 14 – Methodology applied for the parametric study for scenario 2 (storage buried underground)

5.4 Parametric study methodology

In the parametric study, the effects of the variation of the parameters defined above on the storage volume and the $LCOES_{100}$ are investigated. The simulations cover a full year starting on 1st of April. A uniform temperature of 40 °C is assumed as the initial temperature of the storage tank at the beginning of each simulation. The assumed initial temperature distribution becomes virtually irrelevant to this analysis as long as the storage can be fully charged up to the maximum temperature of 90 °C by the end of the summer season. The DHW temperature at the outlet of the uppermost vessel and the SH requirement has been set as the criteria to determine the minimum storage volume required. More specifically, $T_{DHW,out}$ is not allowed to drop below 60 °C at any point in time and the building must be kept above 20 °C throughout the year.

The approach used to conduct the parametric study consists of two steps. In a first step, the minimum storage volume is determined, such that the requirements for DHW and SH are fulfilled. During this step, the value of the relevant parameter is kept constant while the storage volume is varied within a certain range. The minimum volume (V_{min}) is then determined – as shown schematically in Fig. 15 – by interpolating the simulation results such that the minimum value of $T_{DHW,out}$ (reached over the simulated year) is exactly 60°C. In a second step, the optimum value of the investigated parameter is identified by finding the minimum value of $LCOES_{100}$ that is attained over the pre-defined investigated range. The following sub-sections describe the different steps that were undertaken as part of the parametric study. The schematic representation of the methodology used to conduct the parametric study is shown in Fig. 13 (scenario 1) and Fig. 14 (scenario 2).

5.4.1 Characterization of MFC

The performance of the MFC is investigated under combined variation of the target temperature T_{targ} and the solar tilt angle α_{coll}. The aim of this analysis is two-fold: (1) determining the optimum T_{targ} for each α_{coll}, (2) determining $LCOES_{100}$ as a function of α_{coll}. This step of the parametric study is performed in Section 6.2 based on the following parameters and boundary conditions:

- Scenario: 1 (storage integrated inside the building)
- Case: Retrofit
- Location: Bern
- Solar controller: MFC
- T_{targ}: 70 – 110 °C (interval: 10 °C) → **variable parameter**
- α_{coll}: 40 – 75° (interval: 5°) → **variable parameter**
- A_{coll}: 187 m²
- Tank height, h_{tank}: 15 m
- Thermal insulation: Glass wool (GW)
- λ_{ins}: $1.263 \cdot 10^{-4} T - 1.074 \cdot 10^{-3}$ W/mK
- R-value: 7.4 m²K/W (30-cm-thick GW)

5.4.2 Characterization of HFC/LFC and comparison of all controllers

In this step, the performance of the HFC and the LFC is investigated under combined variation of the solar tilt angle α_{coll}. The aim of this analysis is to determine $LCOES_{100}$ as a function of α_{coll} for both controllers. This step of the parametric study is performed in Section 6.3 based on the following parameters and boundary conditions:

- Scenario: 1 (storage integrated inside the building)
- Case: Retrofit
- Location: Bern
- Solar controller: HFC, LFC
- α_{coll}: 40 – 75° (interval: 5°) → **variable parameter**
- A_{coll}: 187 m^2
- Tank height, h_{tank}: 15 m
- Thermal insulation: Glass wool (GW)
- λ_{ins}: $1.263 \cdot 10^{-4} T - 1.074 \cdot 10^{-3}$ W/mK
- R-value: 7.4 m^{2}K/W (30-cm-thick GW)

Following the characterization of all three controllers (MFC, HFC, and LFC), their performance are compared. The aim is to identify the controller leading to the lowest storage volume and thereby to the lowest $LCOES_{100}$. Here, it is assumed that the cost differences of the three controllers associated to the control hardware and software, the circulation pump and piping on the solar circuit is negligible compared to all the other costs associated to the storage, the solar collector, their installation, and the cost penalties associated to the loss of living space and the internal reconstruction of the building.

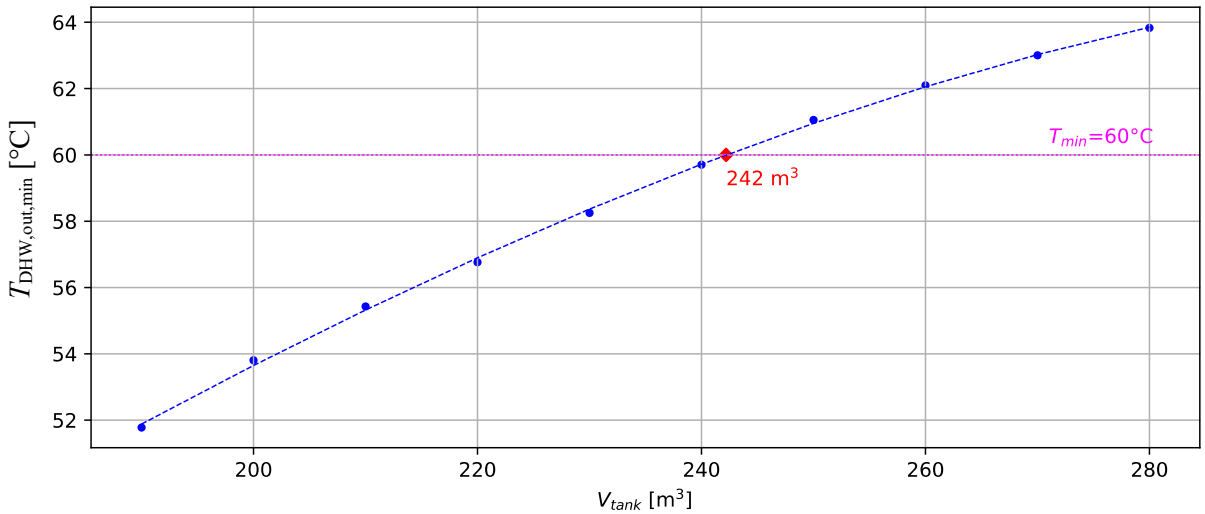

Fig. 15 – Illustration of the interpolation method used to determine V_{min} (242 m^3 in this case). The storage is sized such that the minimum value of $T_{DHW,out}$ reached during the simulated year is 60 °C.

5.4.3 Solar collector area

Here, the influence of the solar collector area on the $LCOES_{100}$ is investigated. The solar tilt angle is set to 45° according to the characteristics of the representative multifamily house chosen for this study (Section 5.1.1). This step of the parametric study is performed in Section 6.4 based on the following parameters and boundary conditions:

- Scenario: 1 and 2
- Cases (scenario 1): - Retrofit
  - New building, footprint affected
  - New building, footprint unaffected
- Location: Bern
- Solar controller: LFC (optimum identified in the previous step)
- α_{coll}: 45°
- A_{coll}: 157 – 237 m², (interval: 10 m²) → **variable parameter**
- Tank height, h_{tank}: 15 m
- Thermal insulation: Glass wool (GW)
- λ_{ins}: $1.263 \cdot 10^{-4} T - 1.074 \cdot 10^{-3}$ W/mK (GW)
- R-value: 7.4 m²K/W (30-cm-thick GW)

5.4.4 Thermal insulation

In this step, the potential of reducing the $LCOES_{100}$ through the use of alternative thermal insulation materials is investigated – baseline is conventional glass wool. The analysis involve varying the material (and thereby its thermal conductivity and cost) and the R-value (given by its thickness). The aim is to identify the combination of material and R-value that leads to the lowest $LCOES_{100}$. In order to allow a direct comparison between different insulation materials and thicknesses, fixed R-values are used. The R-value is defined as $R = \delta/\lambda$. To find the thickness of each insulation material for the corresponding R-value, the thermal conductivity was assumed temperature independent. The constant values of the thermal conductivities were taken at 60 °C and are provided below.

Table 6 shows the insulation thickness of each material with a given R-value. This step of the parametric study is performed in Section 6.5 based on the following parameters and boundary conditions:

- Scenario: 1 (storage integrated inside the building)
- Cases: - Retrofit
  - New building, footprint affected
  - New building, footprint unaffected
- Location: Bern, Zurich
- Solar controller: LFC (optimum identified in previous step)
- α_{coll}: 45°
- A_{coll}: 187 m² (optimum identified in previous step)
- Tank height, h_{tank}: 15 m
- Thermal insulation: GW, XPS, PIR, VIP → **variable parameter**
- λ_{ins} (@60 °C): GW: 41.0 mW/mK
  XPS: 39.2 mW/mK
  PIR : 30.5 mW/mK
  VIP : 12.0 mW/mK
- R-value: 3.7 – 19.6 m²K/W → **variable parameter**

Table 6 – Insulation thickness required to achieve a given *R*-value for the different materials considered.

***R*-value [m²K/W]**	**3.70**	**5.00**	**7.41**	**9.8**	**12.2**	**14.7**	**17.2**	**19.6**
GW [cm]	15.2	20.5	30.4	40.2	50.0	60.3	70.7	80.4
XPS [cm]	14.5	19.6	29.1	38.5	47.8	57.7	67.6	76.9
PIR [cm]	11.3	15.3	22.6	29.9	37.2	44.9	52.6	59.8
VIP [cm]	4.44	6.00	8.89	11.8	14.6	17.6	20.7	23.5

5.4.5 Height of buried storage

The influence of different storage heights are compared to each other. The aim of this analysis is to determine the height that leads to the lowest $LCOES_{100}$. This step of the parametric study is performed in Section 6.6 based on the following parameters and boundary conditions:

- Scenario: 2 (storage buried underground)
- Location: Bern
- Solar controller: LFC (optimum identified in previous step)
- Tank height, h_{tank}: 7 – 15 m (interval: 1 m)
- α_{coll}: 45°
- A_{coll}: 187 m² (optimum identified in previous step)
- Thermal insulation: evacuated powders (double-wall vacuum tank)
- *R*-value[3]: 20 m²K/W

[3] Based on vacuum-insulated storage tanks commercially available [17].

6 Results and discussion

6.1 Overview and discussion model outputs

On the basis of a reference baseline simulation, the following section provides a first insight into the characteristic dynamics of the investigated STES system. The aim is to illustrate the transient behavior of the storage system and identify the key parameters and phenomena that will play a major role in the parametric study. The inputs and boundary conditions used for this reference simulation are:

- Scenario: 1 (in house, retrofit)
- Location: Bern
- Solar installation: Controller = HFC, α_{coll} = 45°, A_{coll} = 187 m^2
- V_{tank}: 250 m^3 (tank height: 15 m)
- Thermal insulation: Glass wool ($\lambda_{ins} = 1.263 \cdot 10^{-4}T - 1.074 \cdot 10^{-3}$ W/mK)
- R-value: 7.4 m^{2}K/W (30-cm-thick GW)

Fig. 16 shows the temperature distribution over the year at five different heights in the storage and the DHW temperature at the outlet of the uppermost vessel ($T_{DHW,out}$). The simulation starts on 1st of April with a uniform tank temperature of 40 °C. The 0H-curve represents the lowest point in the storage. The 1H-curve represents the uppermost point in the storage and is – in this example simulation – virtually identical to $T_{DHW,out}$ throughout the year. In general, these two temperatures can differ when DHW is drawn from the uppermost vessel depending on the temperature distribution along the vessel. The sharp drops in the 0H-curve (e.g. from Nov. till Apr.) are the result of: (i) the low-temperature flow (~25°C) returning from the SH system, and (ii) the inflow of fresh water into the lowermost DHW vessel. In autumn and winter further temperature drops are observed at 0.25 H, which are the result of extensive heat extraction for DHW and SH. Approximately 2.5 months after the start of the simulation, the storage is completely charged at 90 °C from top to bottom. In October, the combined effects of decreasing solar yield and increased heat demand become noticeable. In November, the temperature in the lower part of the tank drops sharply, whereas in the upper half (above 0.5 H) temperatures decrease at a slower rate,

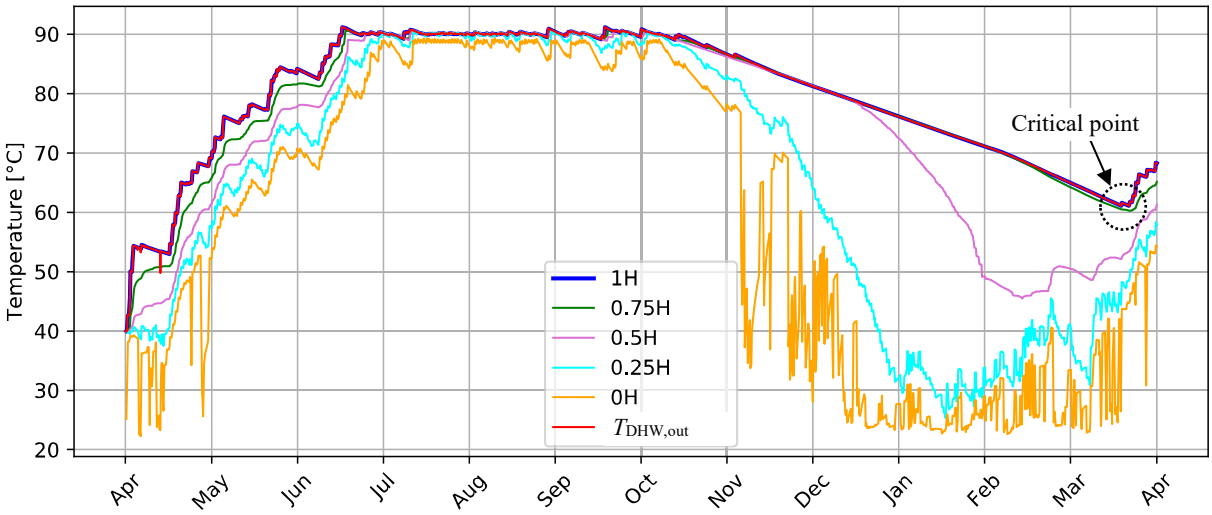

Fig. 16 – Simulated storage temperature profiles and DHW temperature at the outlet of the uppermost vessel ($T_{DHW,out}$). Results correspond to scenario 1 (storage in building). Temperature profiles correspond to five different heights in the tank (0H: bottom of the tank; 1H: top of the tank). The critical point corresponds to the time at which $T_{DHW,out}$ reaches its minimum in the course of the year.

primarily driven by heat losses. Up to mid-December, the building energy requirements are covered by using only the lower half of the storage. Following this period, energy starts to be consumed from the upper half of the storage. At the critical point (i.e. when $T_{\mathrm{DHW,out}}$ reaches its lowest point, in this case between March and April) the storage temperature in the upper section of the tank needs to remain slightly above 60 °C in order to satisfy the DHW requirements. Following the critical point, the temperatures in the storage upper section start rising again as a result of the increasing solar irradiation.

The DHW temperatures at the outlet of each vessel are shown in Fig. 17 over the course of the simulated year. The temperature curves closely follow the storage temperatures shown in Fig. 16. Up to January only the lowest vessel is used for the supply of DHW. The second vessel is then added whereas the top vessel is used to a lesser extent. With this configuration, the temperature of the DHW does not fall below the 60 °C limit, indicating that the tank is large enough to meet the DHW requirements.

The use of the four HEX and their inlet temperatures is shown in Fig. 18. The inlet temperature of the uppermost 'active' (i.e. not bypassed) HEX corresponds to the temperature of the HTF delivered by the solar collectors ($T_{\mathrm{coll,out}}$). Up to end-June, the harvested solar energy is transferred to the storage via all four heat exchangers – over this period, the storage is progressively charged from top to bottom. A full charge is reached by the beginning of July, after which the storage is able to absorb heat only to a lesser extent – primarily through the two lowest heat exchangers. As a result of the decreasing solar irradiation and thus the lower $T_{\mathrm{coll,out}}$, the heat delivered by the solar collectors after October is typically supplied to the storage by means of the lowest heat exchangers. Note however that this is strong dependent on the solar collector control strategy – a matter that will be discussed in detail in Section 6.3.

The characteristics of the hot water extraction for the SH system are shown in Fig. 19. The figure allows identifying the points in time during which a given port was active as well as the temperature of the extracted (POR 2 – POR 4) and returned (POR 1) flows. The solid line represents the room temperature. The simulation results reveal that up to November the SH demand of the building was entirely covered by means of the heat losses of the storage as none of the ports showed any activity up to that point in time. The floor heating is then operated actively (i.e. by extracting water from the storage) when the heat losses from the storage are not large enough – this is the case for the period starting in November. Most of the water flow required for space heating is provided by POR 2. POR 3 is only used in Jan and Feb, whereas POR 4 is never used.

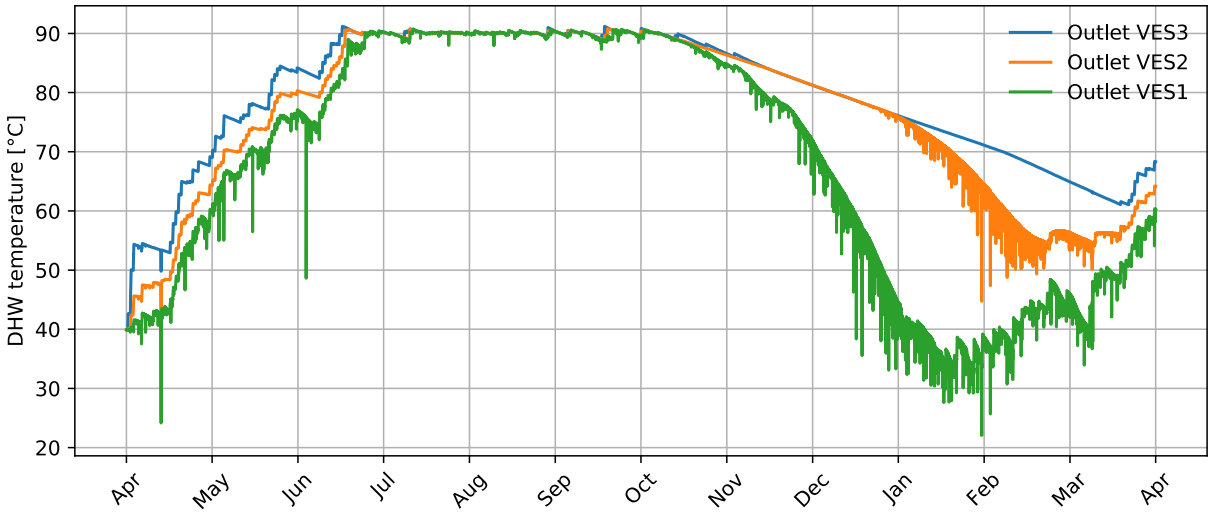

Fig. 17 – Simulated DHW temperature profiles of the reference STES for scenario 1 (storage in building). The profiles correspond to the DHW outlet temperature of the three vessels (VES1: lowermost vessel, VES3: uppermost vessel, see Fig. 2 and Fig. 5).

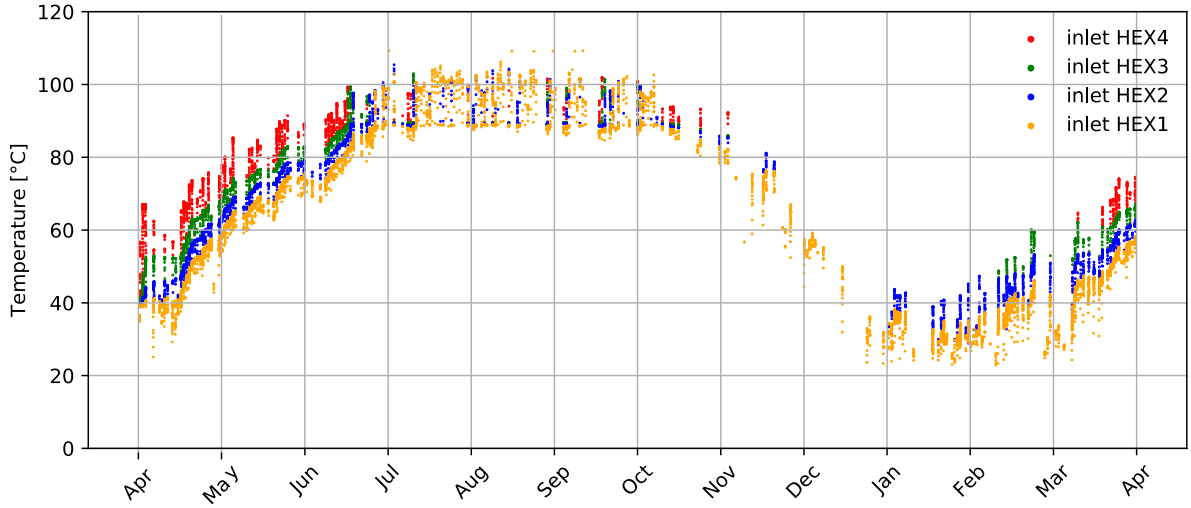

Fig. 18 – Simulated heat exchangers temperatures of the reference simulation. The dots correspond to the inlet temperature of the four heat exchangers.

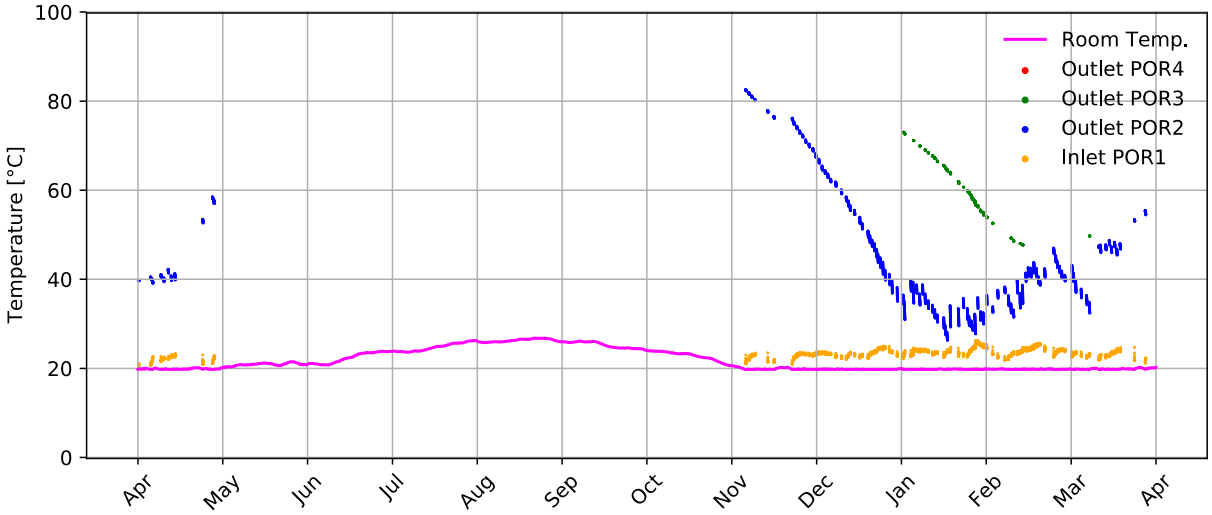

Fig. 19 – Simulated port temperatures and room temperature of the reference simulation. The dots correspond to the inlet (POR 1) and outlet (POR 2 – POR 4) temperatures of the four ports. The location and function of the ports is shown in Fig. 6.

Fig. 20 shows the following temperature curves: (1) hourly-averaged outside temperature (orange curve), (2) daily-averaged outside temperature (red curve), and (3) room temperature (blue curve). The simulation results show how the storage and the control system are able to effectively regulate the room temperature to 20 °C. In terms of the energy breakdown and the calculation of the $LCOES_{100}$, the following rule is applied: for scenario 1, there are so called "usable" energy losses from the storage into the building. These are energy losses that contribute to space heating and therefore replace a part of the energy supplied via the floor heating system. To distinguish between "usable" energy losses and actual energy losses, an adiabatic simulation was performed to determine the total energy demand for SH.

The breakdown of energy use over the simulated year is shown in Fig. 21. The total energy collected by the solar collectors for this simulation configuration was 201 GJ. Out of this, 76 GJ (38%) was used for the provision of DHW. Throughout the year, the storage tank loses a total of 52 GJ (26%) heat into its surroundings. Of these, 31 GJ (60% of the heat losses) is considered usable heat to cover the SH demand, whereas the remaining 21 GJ are regarded as true heat losses. Thus, it can be said that the system has a total heat loss of 10%. The additional energy required for satisfying the SH demand is 51 GJ. Based on this results, the SH requirement of the house is estimated at 25 kWh/m²a. At the end of the year, the remaining energy content of the storage (as compared to the initial condition of 40 °C) is round 11%. Even if multiple years were simulated, this share would remain virtually unaffected given the fact that the temperature distribution at the end of the summer season (90 °C throughout the tank) would remain the same. For this reference simulation, the energy balance error was only 0.4%.

The cost breakdown for the reference simulation (storage integrated inside an existing building) is shown in Fig. 22. The definition of the individual cost categories has been defined in Section 5.2. The total costs for the construction, installation, and integration of the STES system (incl. the solar thermal system and installation) in the house was estimated at round 1.2 Mio. CHF. The largest share of the costs (54%) results from the loss of living space. Internal reconstruction of the building – to allow the integration of the storage – accounts for 20% of the total investment costs. The solar collectors and the thermal storage (incl. their installation) account to 27% of the total costs (320 kCHF).

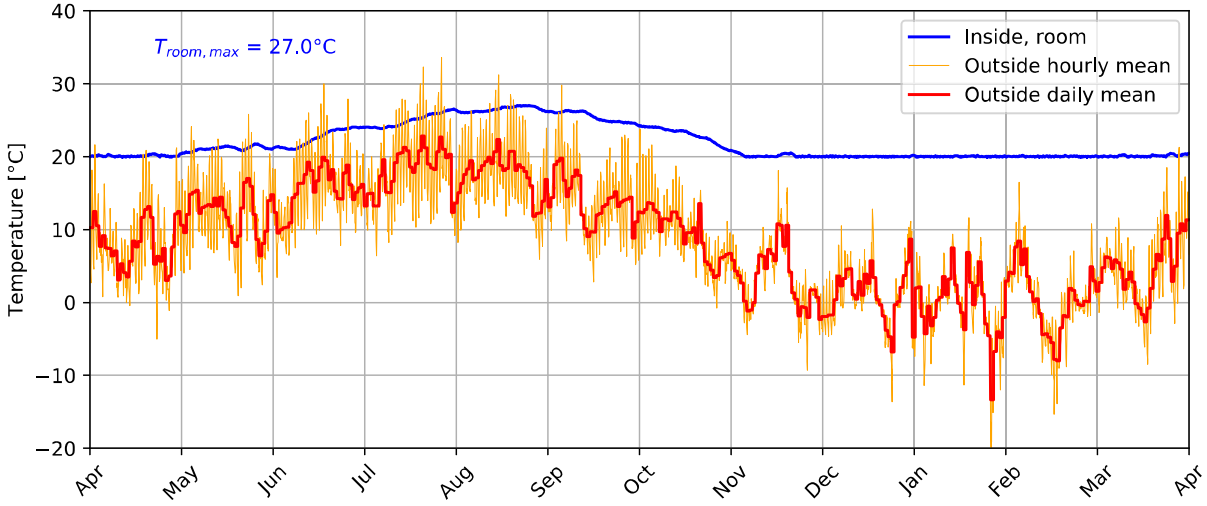

Fig. 20 – Simulated room temperature of the reference STES for scenario 1 (storage in building). Results are shown for a full simulated year. Hourly and daily means of the ambient temperature are shown as a reference.

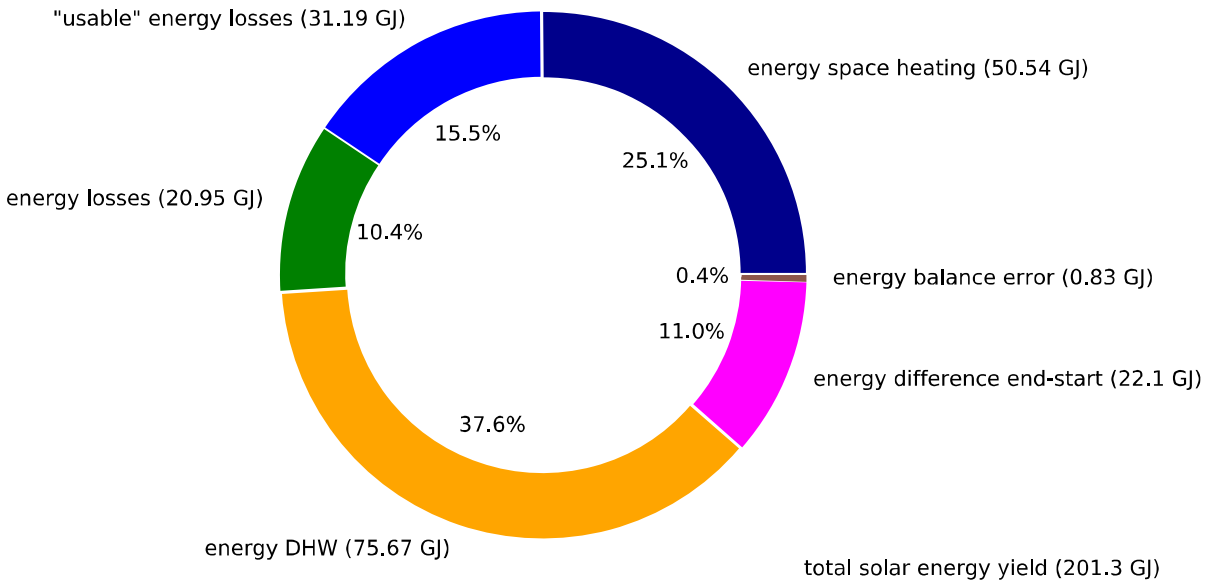

Fig. 21 – Energy distribution of the reference STES for scenario 1 (storage in building). Results are shown for a full simulated year.

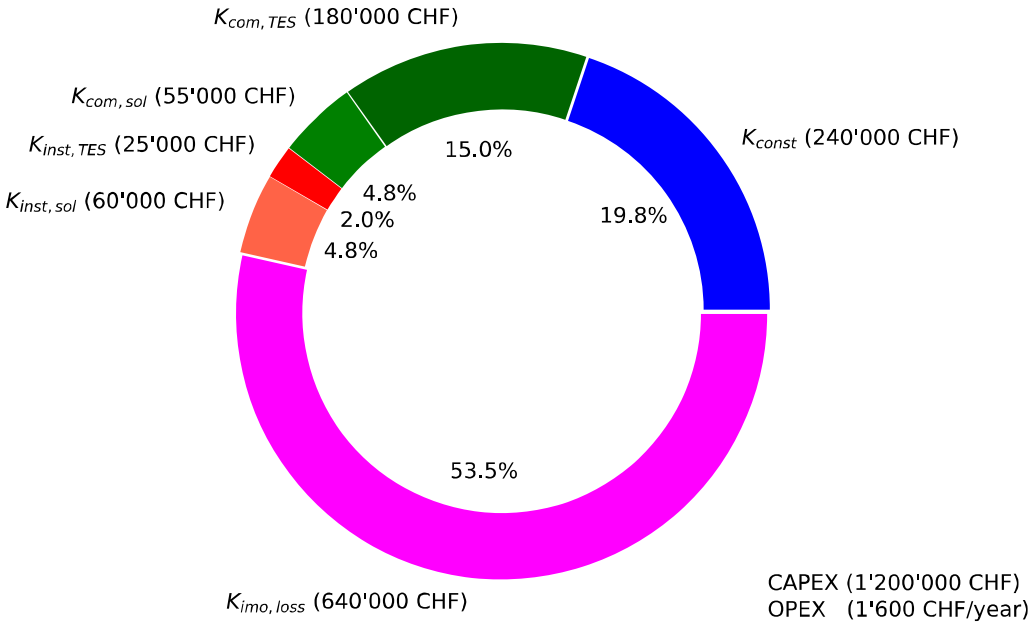

Fig. 22 – Cost breakdown of the reference simulation (scenario 1, retrofit). K_{com}: cost of components; K_{ins}: cost for the installation of the components; K_{const}: cost for the internal reconstruction of the building (only relevant for the retrofit case in scenario 1); $K_{imo,loss}$: costs due to the loss of living space.

6.2 Characterization of MFC

The first step of the parametric study examines the influence of α_{coll} and T_{targ} on the performance of the MFC. This step of the parametric study is performed according to the parameters and boundary conditions described in Section 5.4.1. The performance of the controller is measured in terms of the minimum storage volume required (V_{min}) and the $LCOES_{100}$ – the latter is the decisive criterion, while V_{min} serves as an indication of the relative impact of the controller. The different control strategies were described in Section 2.3.1. As shown in Fig. 23, the lowest $LCOES_{100}$ is achieved when setting $T_{targ} = 90$ °C. This optimum is presumed to result from the tradeoff between (i) the temperature difference between HTF and storage medium (water) for an effective heat transfer rate, and (ii) the efficiency of the solar collectors (which decreases with increasing collector temperature).

Table 7 shows the required minimum volume and $LCOES_{100}$ for different tilt angles. The values in parentheses show the relative cost and volume reduction that can be attained as compared to the baseline case ($T_{targ} = 90$ °C and $\alpha_{coll} = 45°$). At $T_{targ} = 90$ °C (green curve in Fig. 23) the $LCOES_{100}$ and V_{min} can be reduced 8% and 11% if the tilt angle is increased from 45° to an optimum of 65° – at the optimum point $LCOES_{100}$ is round 1.1 CHF/kWh. The optimum angle of 65° is the result of the increased solar yield of the solar collectors during the winter season (particularly during mid-Dec – mid-Feb) when the heat demand is the highest. The altitude of sun from mid-Dec to mid-Feb is between 20 and 30° which is consistent with the optimal tilt angle of 65° found in this study. These results are also consistent with [14], which indicates that the best solar tilt angle for maximum solar yield during winter is 60°, whereas the best angle for the entire year is 42°.

Regardless of the optimum angle found, $\alpha_{coll} = 45°$ will be taken for the next steps of the parametric study as this is considered representative of the roof angle of existing buildings of the reference building period (see Section 5.1.1). Taking a larger tilt angle (e.g. $\alpha_{coll} = 65°$) would be – in the framework of this study – an unrealistic retrofit solution to be installed directly on the roof of these type of buildings.

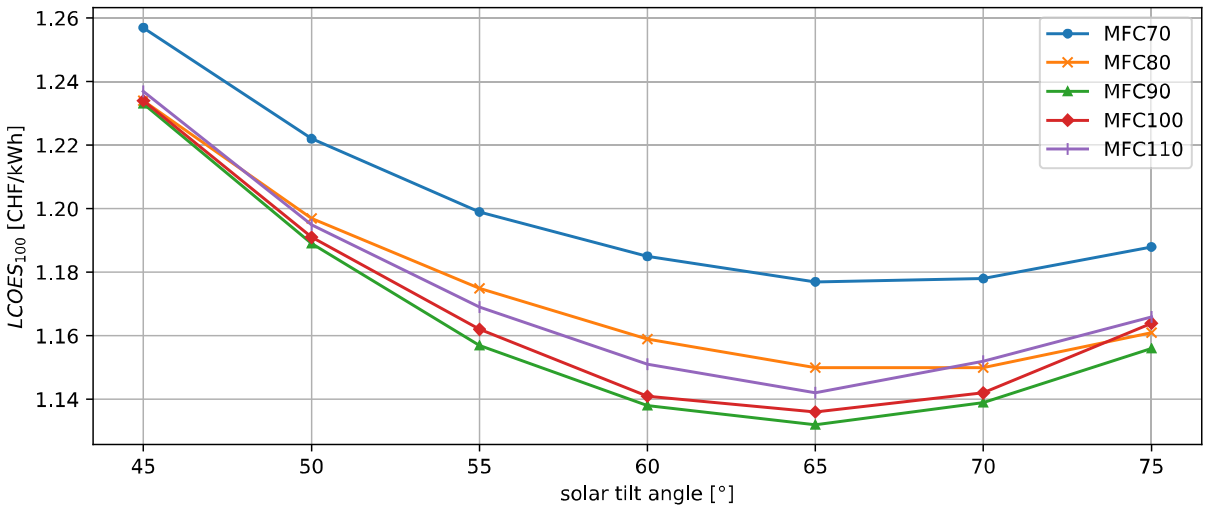

Fig. 23 – $LCOES_{100}$ of MFC with various target temperatures for tilt angles between 40° and 75°. In the legend, the number next to 'MFC' denote the corresponding value of T_{targ} in °C.

Table 7 – Minimum storage volume and $LCOES_{100}$ for MFC (green curve in Fig. 23 and Fig. 24), HFC and LFC. The values in parentheses show the relative cost and volume reduction that can be achieved by changing α_{coll} as compared to the baseline case ($\alpha_{coll} = 45°$).

	Solar tilt angle →	45°	55°	65°	75°	
HFC	V_{min}	242	229 (5%)	226 (7%)	237 (2%)	[m³]
	$LCOES_{100}$	1.52	1.46 (4%)	1.45 (5%)	1.50 (1%)	[CHF/kWh]
MFC	V_{min}	184	168 (7%)	163 (11%)	168 (7%)	[m³]
	$LCOES_{100}$	1.23	1.16 (6%)	1.13 (8%)	1.16 (6%)	[CHF/kWh]
LFC	V_{min}	170	157 (8%)	151 (11%)	153 (10%)	[m³]
	$LCOES_{100}$	1.17	1.11 (5%)	1.08 (8%)	1.08 (8%)	[CHF/kWh]

6.3 Characterization of HFC/LFC and comparison of all controllers

The HFC and LFC were characterized as a function of α_{coll} and compared to the performance of the MFC described above. This step of the parametric study is performed according to the parameters and boundary conditions described in Section 0. As shown in Fig. 24, the lowest $LCOES_{100}$ is achieved with the LFC (1.2 CHF/kWh), whereas the HFC leads to the highest $LCOES_{100}$ (1.5 CHF/kWh) – both values given for the reference $\alpha_{coll} = 45°$. The MFC performed somewhere in between – the physical reason behind it will be discussed below.

Table 7 shows V_{min} and $LCOES_{100}$ for all three controllers as a function of α_{coll}. The values in parentheses indicate the relative cost and volume reduction that can be achieved by changing α_{coll} as compared to the 45° reference baseline. Regardless of the controller, the lowest $LCOES_{100}$ can be achieved at $\alpha_{coll} = 65°$ – thereby a reduction of 11% and 8% can be attained for V_{min} and $LCOES_{100}$, respectively. Furthermore, in terms of V_{min}, the simulation results indicate that switching from HFC to LFC would allow the required volume to be reduced by 30% – from 242 down to 170 m³.

A comparative analysis of the three controllers reveal that the reason behind the specific performance characteristics of a given controller directly relates to the exergy distribution it effects within the storage. This exergy distribution relates directly to the storage temperature stratification, which is shown in Fig. 25 for all three controllers (top: HFC, middle: MFC, low: LFC). The results shown in Fig. 25 – 27 correspond to three simulations conducted with the following parameters, where only the solar controller has been changed:

- Scenario: 1 (storage integrated inside the building)
- Location: Bern
- Solar installation: $\alpha_{coll} = 45°$, $A_{coll} = 187$ m²
- V_{tank}: 180 m³
- Tank height, h_{TES}: 15 m
- Thermal insulation: Glass wool ($\lambda_{ins} = 1.263 \cdot 10^{-4}T - 1.074 \cdot 10^{-3}$ W/mK)
- R-value: 7.4 m²K/W (30-cm-thick GW)

Note that based on the results provided in Table 7, a storage volume of 180 m³ is only large enough with the LFC – the other controllers would fail to satisfy the demand for DHW and/or SH. In Fig. 25, the curves 1H and 0.75H represent the most important temperature curves as they are directly associated to the last reserve of the storage to produce DHW. The window between February and April represents the critical period during which this reserve reaches its minimum. While both 1H and 0.75H-curves remain above 60 °C with the LFC, the MFC fails to stabilize the 0.75H-curve and thus to satisfy the DHW requirement ($T_{DHW,out}$ = 60 °C). Note that $T_{DHW,out}$ drops below 60 °C with the MFC – between March

and April – as a result of water being drawn from the uppermost vessel. The HFC on the other hand fails to stabilize both the temperature at 1H and 0.75H and as a result also fails to satisfy the DHW requirement – by mid-February the 1H-curve has already fallen below the 60 °C limit. Whether the temperatures in the upper section of the tank can be sustained or not above the 60 °C threshold depends strongly on two aspects: (1) how the storage is charged, and (2) how it is discharged by the SH system – two aspects that are closely interdependent. The characteristics of the charging process are primarily driven by the solar thermal collector controller as this determines the temperature attained at the outlet of the solar collectors ($T_{coll,out}$) and ultimately the temperature at the inlet of the HEX of the storage. Fig. 26 shows the flow temperatures at the inlet of the HEX attained with each of the three controllers (top: HFC, middle: MFC, low: LFC). The HFC is characterized by temperatures that are strongly dependent on the solar irradiation conditions. Temperatures of around 100 °C are only reached during summer when solar irradiation is very high. In winter, when the high-temperature reserve of the storage is nearly depleted, the controller fails to supply heat at the temperatures required to replenish this reserve – this is identified by the fact that the uppermost HEX (HEX 4, red dots) is active only sporadically between January and March. The MFC, on the other hand, is characterized by higher and more stable solar collector output temperatures ($T_{coll,out}$) as a result of the active control of the flow rate in the solar circuit aiming at $T_{coll,out} = T_{targ} = 90$ °C. This results in a stronger thermal stratification in the storage, for example as compared to the LFC. The strong stratification that results from using the MFC result in a sharp drop in the storage temperature at 0.75H by the end of January. This drop is the consequence of consuming the high-temperature reserve in the upper section of the storage to cover the SH demand – in the absence of suitable temperatures in the lower part of the tank, the controller has no alternative, but to extract hot water from the uppermost port (POR 4) – this is illustrated in Fig. 27. The frequency of the red dots (POR 4) observed with the MFC is significantly higher than the frequency obtained with the LFC or the HFC. Extracting water at high temperatures for the SH systems results in significant irreversibilities due to mixing of water flows at different temperatures (given that $T_{flow} \sim 35$ °C) and thus in a significant exergy destruction rate. The ultimate result is a quick depletion of the high-temperature reserve in the upper section of the storage and a subsequent failure to meet the DHW requirement. As revealed by Fig. 25–27, the LFC seems to represent the ideal compromise between providing high-temperature heat for DHW and mid-temperature heat for the SH demand. Note that the conclusions derived in this section are the same for scenario 2 given that minimizing the storage volume automatically leads to the minimum $LCOES_{100}$ – this is the case because the cost differences associated to the controllers themselves are neglected in this analysis (see Section 2.3.1).

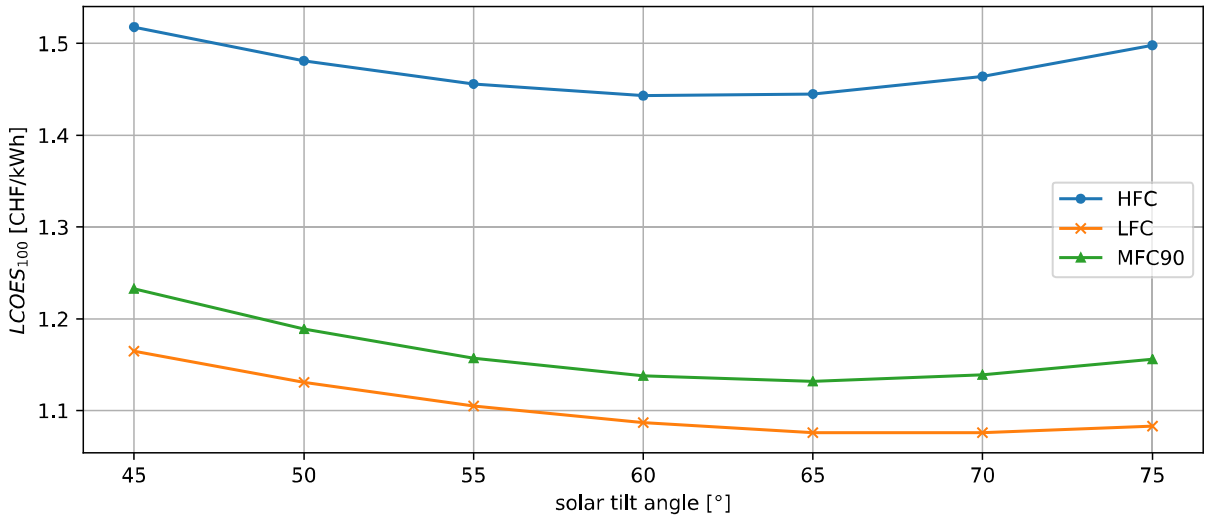

Fig. 24 – $LCOES_{100}$ obtained when using the HFC, LFC and MFC (with $T_{targ} = 90$ °C) for tilt angles between 45° and 75°.

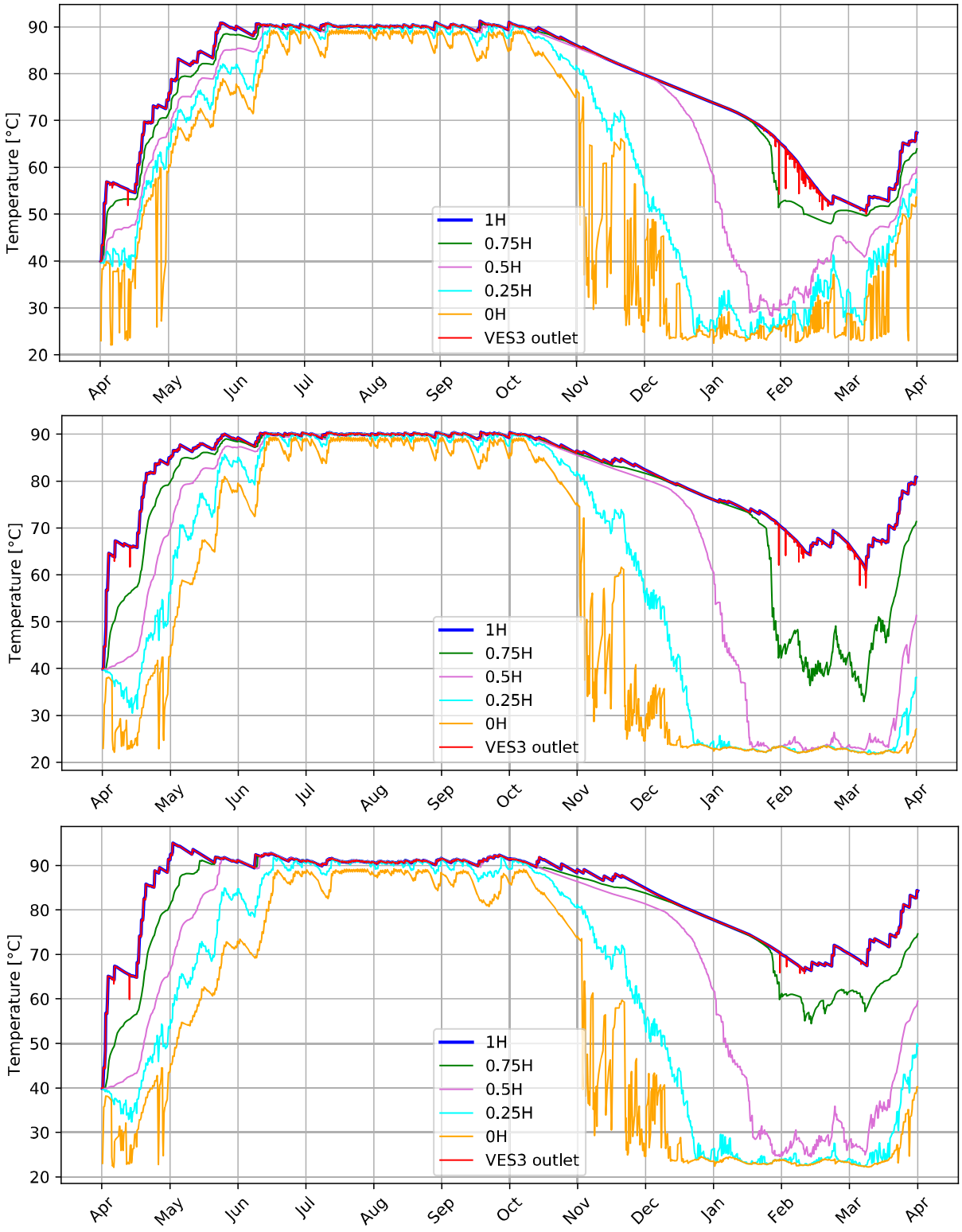

Fig. 25 – Simulated storage temperature profiles for the different solar collector controllers. HFC (top), MFC (middle), LFC (bottom). 1H = storage top, 0H = storage bottom, VES3 outlet = $T_{DHW,out}$ (top vessel outlet temperature)

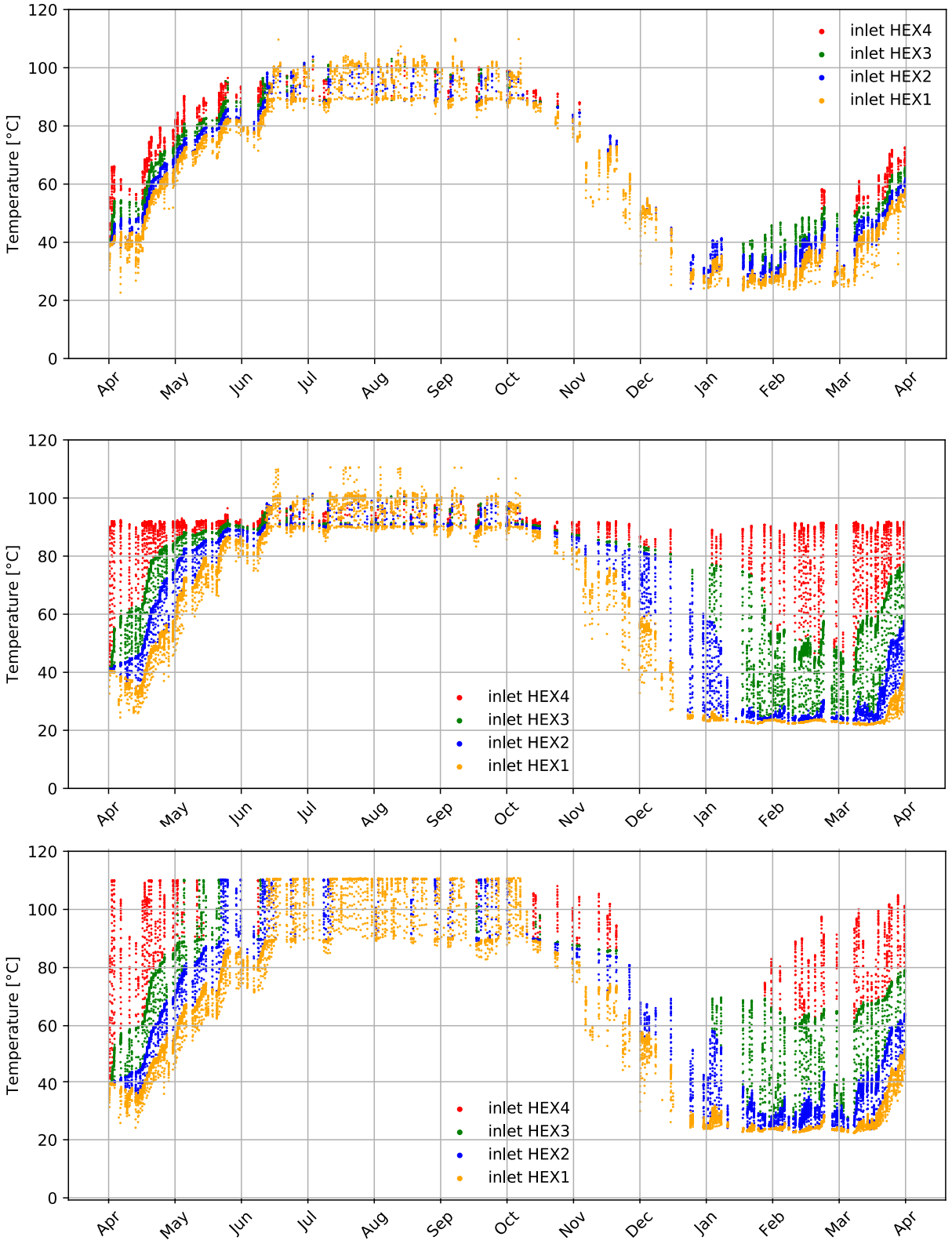

Fig. 26 – Simulated HEX inlet temperatures for the different solar collector control strategies. HFC (top), MFC (middle), LFC (bottom). HEX1 = lowermost HEX, HEX4 = uppermost HEX.

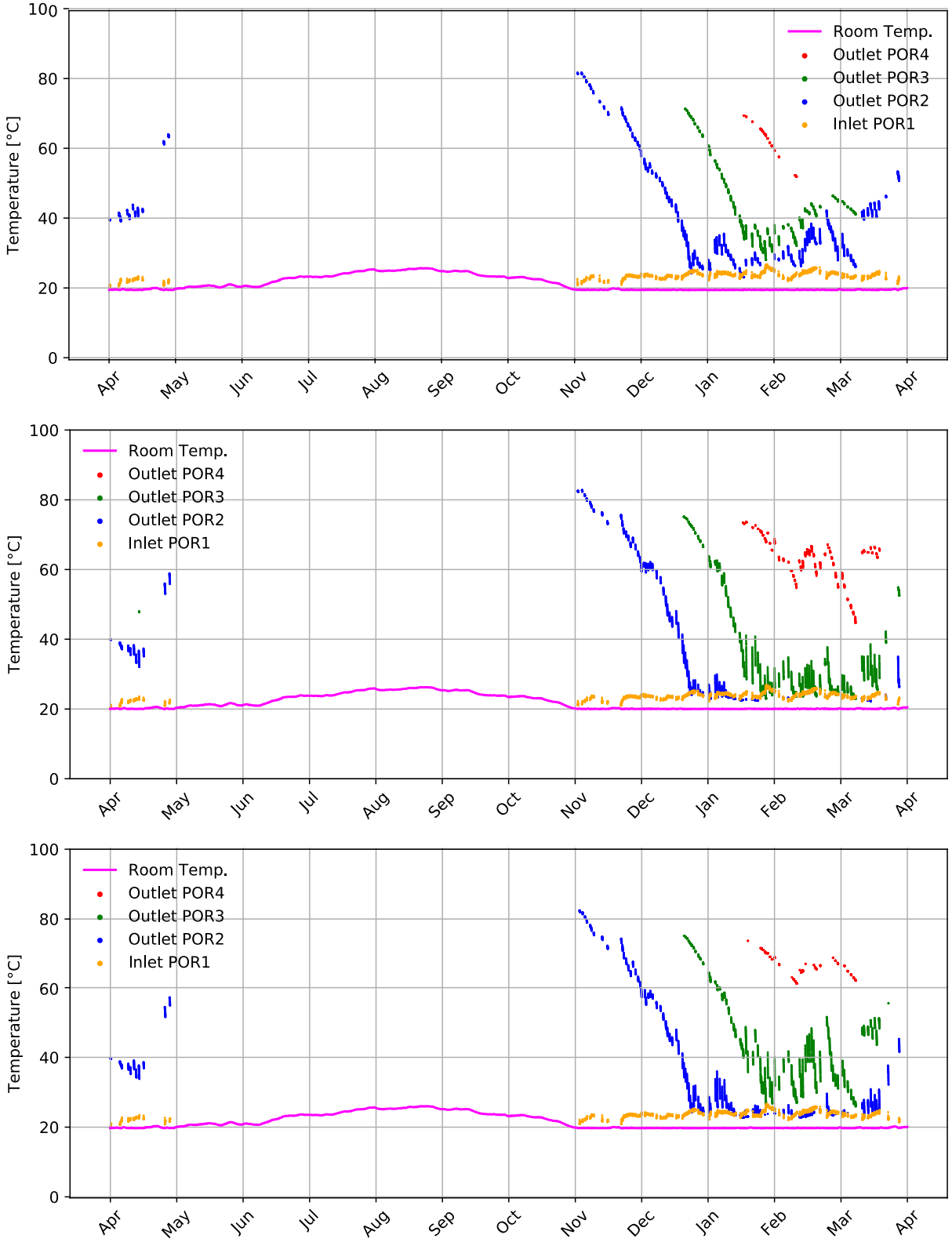

Fig. 27 – Simulated port temperatures for the different solar collector control strategies. HFC (top), MFC (middle), LFC (bottom). POR1 = lowermost POR (return to the tank), POR4 = uppermost POR.

6.4 Solar collector area

6.4.1 Scenario 1 (storage in building)

The size of the solar collector area (A_{coll}) has a significant impact on the required storage volume and ultimately on the $LCOES_{100}$. The smaller the solar collector area, the larger the required storage volume and vice versa. This relationship is limited by the following conditions: (1) the solar collector area can only be reduced to the point where the solar yield is large enough to charge the storage above 60 °C (required to fulfill the DHW requirement), and (2) the storage volume can only be reduced to the point where the stored heat is enough to bridge the gap at times when there is no solar irradiation (e.g. overnight and cloudy/winter days with no solar yield).

This step of the parametric study is performed according to the parameters and boundary conditions outlined in Section 0. Fig. 28 shows the minimum required storage volume and the $LCOES_{100}$ as a function of the solar collector area for the following three cases (see Section 2.1 for case descriptions):

1. Retrofit (RF)
2. New building, footprint affected (NB-FA)
3. New building, footprint unaffected (NB-FU)

While V_{tank} clearly decreases with increasing A_{coll}, the effect of A_{coll} on V_{tank} and $LCOES_{100}$ strongly depends on the specific case under consideration. In the RF case (storage integrated inside an existing building), the costs savings associated to the smaller storage outweighs the increased investment costs associated to the larger solar collector installation. A smaller storage volume has in this case a three-fold effect: (1) reduced cost of the storage tank itself, (2) reduced penalty costs associated to the loss of living space, and (3) reduced penalty costs associated to the internal reconstruction of the building. To illustrate the impact of A_{coll}, note that increasing the solar collector area by 50% (from 160 to 240 m^2) in the RF case would lead to a reduction in V_{tank} and $LCOES_{100}$ of 35% and 25%, respectively. Here, A_{coll} has been increased beyond the available roof area of the reference building with the aim of illustrating the cost reduction potential associated to this parameter.

The impact of A_{coll} on $LCOES_{100}$ is significantly smaller for the case NB-FA, as the penalty costs are reduced in this case to the opportunity costs of the reduced footprint only. Increasing A_{coll} from 160 to 240 m^2 would lead to a reduction in $LCOES_{100}$ of 15%. Note that the $LCOES_{100}$ in the case NB-FA is round 50% of that of the RF case – this as a result of avoiding the large penalty costs associated to the loss of living space and the internal reconstruction of the building.

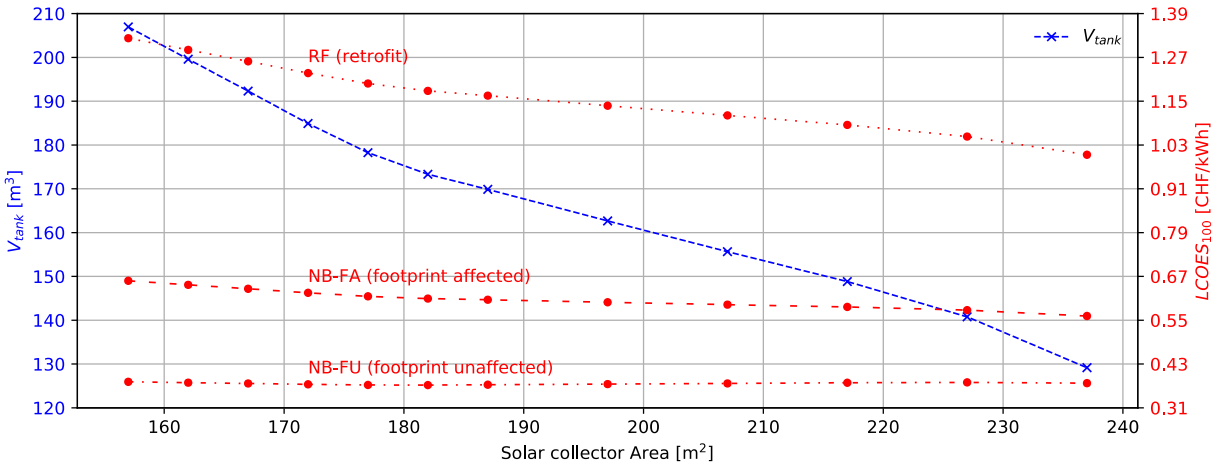

Fig. 28 – Minimum required storage volume (left axis) and $LCOES_{100}$ (right axis) as a function of the solar collector area for all cases "Retrofit" (RF) "New building, footprint affected" (NB-FA) and "New building, footprint unaffected" (NB-FU).

Finally, in the case NB-FU, the $LCOES_{100}$ remains virtually unaffected by the variation of A_{coll}. In this case, the cost savings associated to the smaller storage is balanced by the additional costs of the solar collector installation, such that the total costs remain essentially constant. This result provides an important insight: for new buildings (especially with an unaffected footprint), the cost balance between solar installation and storage provides valuable flexibility for adjusting the solar installation area depending on the available roof area without affecting the system costs.

6.4.2 Scenario 2 (storage underground)

Analogous to the previous section, a parametric study was conducted to investigate the optimum combination of storage volume and solar collector area leading to the minimum $LCOES_{100}$. Although there is no loss of living space in scenario 2, the significant costs associated to the excavation of the soil leads to the same trend observed for the retrofit case of scenario 1: the lowest $LCOES_{100}$ is attained by maximizing A_{coll} while minimizing the storage volume. For scenario 2, $LCOES_{100}$ can be reduced by round 8% (from 0.78 down to 0.72 CHF/kWh) when increasing A_{coll} – from 160 to 190 m^2 – by 20%.

6.5 Thermal insulation

In this section, the potential of reducing the $LCOES_{100}$ through the use of alternative thermal insulation materials is investigated for scenario 1 – baseline is conventional glass wool. This step of the parametric study is performed according to the parameters and boundary conditions described in Section 5.4.4.

The thermal insulation serves two functions: (i) reducing the heat losses such that the SH and DHW requirements are fulfilled, and (ii) avoiding overheating of the building in summer. In relation to the latter, Fig. 29 shows the maximum room temperature attained during summer as a function of the *R*-value of the thermal insulation. As a reference, the right axis shows the thickness of glass wool (GW) required to achieve the corresponding *R*-values. At an insulation thickness of 80 cm, the maximum room temperature during summer would be essentially the same as if the storage would be placed outside the building (24 °C). Reducing the insulation thickness to 50 cm is expected to result in a temperature rise of less than 1 °C. Reducing the thickness further may result in a significant temperature increase – at a thickness of about 10 cm the room temperature could already exceed the 30 °C limit. Limiting the temperature rise to 2 °C would require a thickness of about 30 cm of GW (*R*-value = 7.4 m^2K/W). The required insulation thickness is thus dependent on the comfort penalties and the eventual additional costs that may result from the need for active cooling during the summer period. Note that these are indicative results as the simplified building model considers only two zones: (1) the shaft in which the storage is incorporated, and (2) the space around the shaft (i.e. the actual living area).

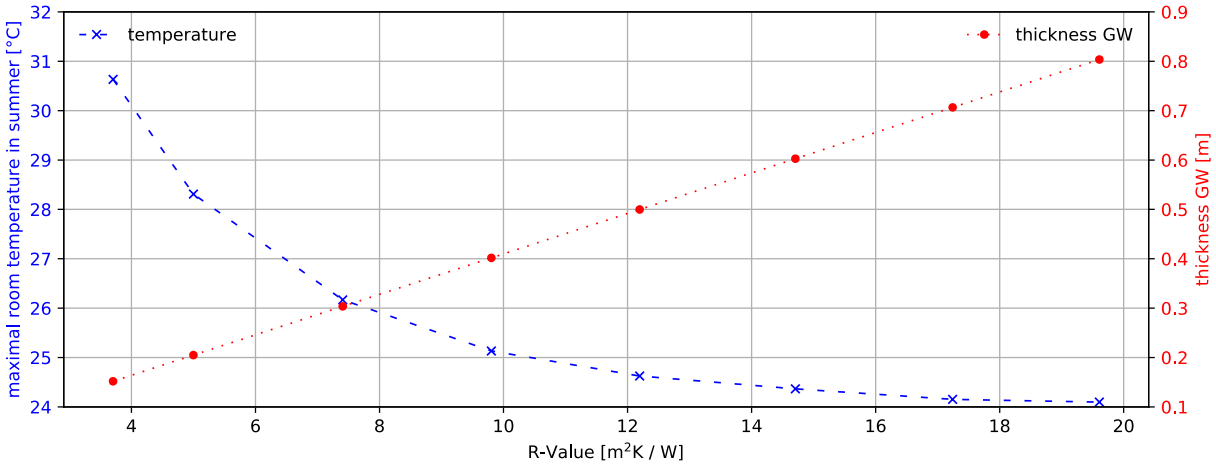

Fig. 29 – Maximal room temperature attained in summer as a function of the *R*-value of the thermal insulation. The right axis shows the thickness of GW required to achieve the corresponding *R*-value.

In terms of the potential for cost reduction, Figs. 30 – 33 show the $LCOES_{100}$ for all three cases of scenario 1 (left axis) along with the living space occupied by the storage (right axis) as a function of the *R*-value. The figures show the results for all thermal insulation materials investigated, namely GW (Fig. 30), XPS (Fig. 31), PIR (Fig. 32) and VIP (Fig. 33). For a given temperature difference, the heat losses of the storage are solely a function of the *R*-value. Hence, the minimum required storage volume is the same for the given *R*-value regardless of the material used. However, due to the difference in thermal conductivity of the various insulation materials, the *total* volume occupied by the storage (i.e. effective storage volume plus insulation) changes with the material. Due to the low thermal conductivity of VIP, for example, storages equipped with VIP lead to the least loss of living space. At an *R*-value of 10 m^2K/W, using VIP instead of GW would allow saving about 20 m^2 of living space.

The trends of the $LCOES_{100}$ curves are similar for all investigated thermal insulation materials. For the cases in which the storage is integrated in a new building (NB-FA and NB-FU), variation of the insulation thickness seems to have virtually no effect on the $LCOES_{100}$. This is presumably because the cost savings associated to a smaller storage (as a result of increased insulation thickness) are compensated by the additional costs associated to the thermal insulation itself. In the retrofit case (RF), on the other hand, there seems to be an economic optimum for the insulation thickness. A thin insulation layer leads to the need for a larger storage (in order to compensate for the increased heat losses), which in turn results in a higher $LCOES_{100}$. With increasing insulation thickness (increasing *R*-value) the required storage volume is reduced and with it the $LCOES_{100}$ – up to an optimum at which $LCOES_{100}$ reaches its minimum. A further increase of the *R*-value would have only a marginal effect on the storage volume, which no longer outweighs the cost associated to the additional thermal insulation material. In the case NB-FU, storage tanks with a GW insulation of 40 cm exhibit the lowest $LCOES_{100}$ at 0.37 CHF/kWh. In the case NB-FA, the lowest $LCOES_{100}$ (0.60 CHF/kWh) is reached when the storage is insulated using PIR insulation of 22 cm.

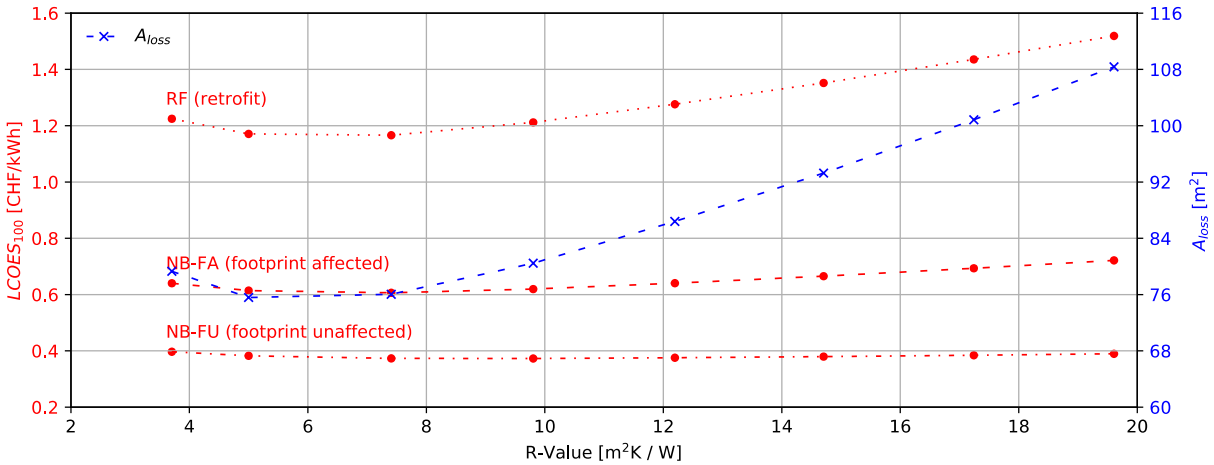

Fig. 30 – $LCOES_{100}$ for all three cases of scenario 1 (storage integrated in the building) as a function of the *R*-value of the thermal insulation. Thermal insulation: glass wool (GW). The right axis shows the extent of living space lost as a result of placing the storage tank inside the building.

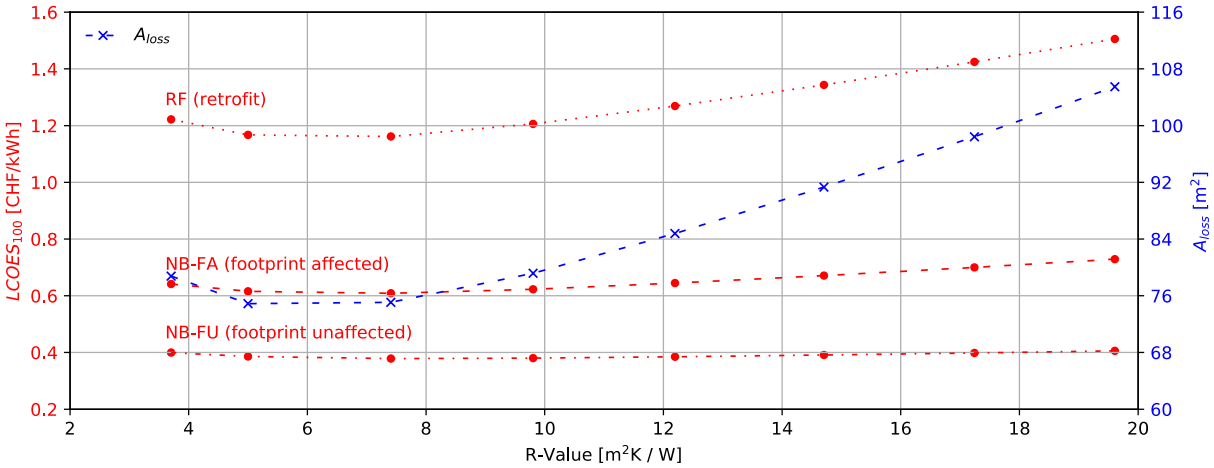

Fig. 31 – $LCOES_{100}$ for all three cases of scenario 1 (storage integrated in the building) as a function of the *R*-value of the thermal insulation. Thermal insulation: XPS. The right axis shows the extent of living space lost as a result of placing the storage tank inside the building.

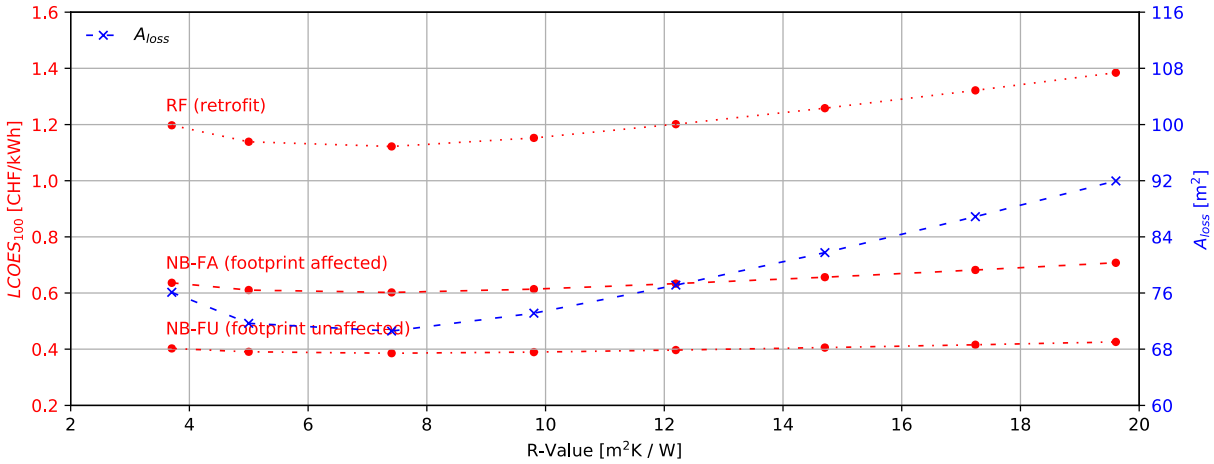

Fig. 32 – $LCOES_{100}$ for all three cases of scenario 1 (storage integrated in the building) as a function of the *R*-value of the thermal insulation. Thermal insulation: PIR. The right axis shows the extent of living space lost as a result of placing the storage tank inside the building.

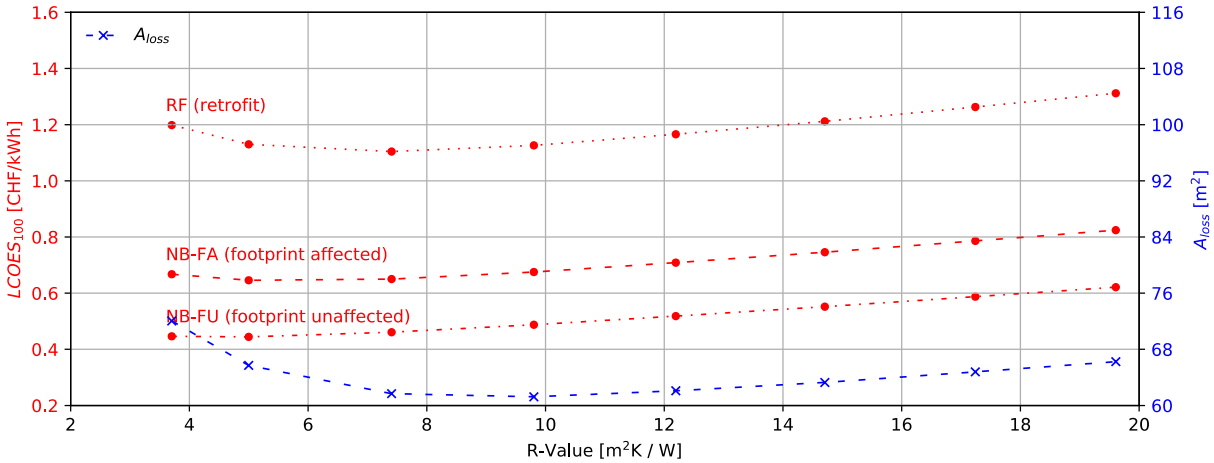

Fig. 33 – $LCOES_{100}$ for all three cases of scenario 1 (storage integrated in the building) as a function of the *R*-value of the thermal insulation. Thermal insulation: VIP. The right axis shows the extent of living space lost as a result of placing the storage tank inside the building.

In terms of the retrofit case, Fig. 34 shows the $LCOES_{100}$ and the loss of living space for the four investigated thermal insulation materials as a function of the *R*-value. Table 8 shows the lowest $LCOES_{100}$ that can be achieved with each material and the corresponding loss of living space. As a result of the high penalty costs associated to the loss of living space and the reconstruction costs of the building, the lowest $LCOES_{100}$ is reached in this case when using VIP. The simulation results indicate that using a 9 cm layer of VIP would lead to a $LCOES_{100}$ of about 1.10 CHF/kWh and would allow saving about 14 m^2 of living space as compared to the use of GW. As compared to VIP, PIR foams can offer a more reliable solution because of the uncertainties associated to the irreversible performance degradation of VIP [17]. As shown in Table 8, the use of PIR would lead to a $LCOES_{100}$ similar to that of VIP and could allow a small cost reduction of about 4% as compared to the use of GW.

In general, the small cost benefit offered by VIP and PIR – as compared to glass wool – would probably not justify the additional complexities and uncertainties associated to these alternative materials. Although PIR can offer a reliable solution (in terms of its long-term thermal stability), its main disadvantage is associated to the challenge of ensuring a proper installation (i.e. establishing a good contact between the material and the tank wall) in order to avoid thermal bridges. This might require for example the use of curved foams tailored to the tank geometry, which in turn could lead to an increase in the material and installation costs.

To investigate the influence of the selected location on the results of this study, additional simulations were conducted using Zurich as the reference location – the corresponding results are shown in Table 9 and Fig. 35. The latter shows the $LCOES_{100}$ and the loss of living space for the four investigated thermal insulation materials as a function of the *R*-value. Note that results are shown for *R*-values above 5.0 m^2K/W as compared to the lower bound of 3.7 m^2K/W for Bern (Fig. 34). This is the result of the difference in the weather conditions, which require a minimum *R*-values of 5.0 m^2K/W in Zurich to allow fulfilling the requirements for SH and DHW. As a result of the higher cost of living space in Zurich (twice as high as that of Bern), the $LCOES_{100}$ is on average 40% higher. Similar to the conclusions drawn for Bern, the lowest $LCOES_{100}$ for the RF case is reached when using VIP. As shown in Table 9, using VIP would lead to a $LCOES_{100}$ of 1.75 CHF/kWh and would allow saving about 14 m^2 of living space as compared to the use of GW.

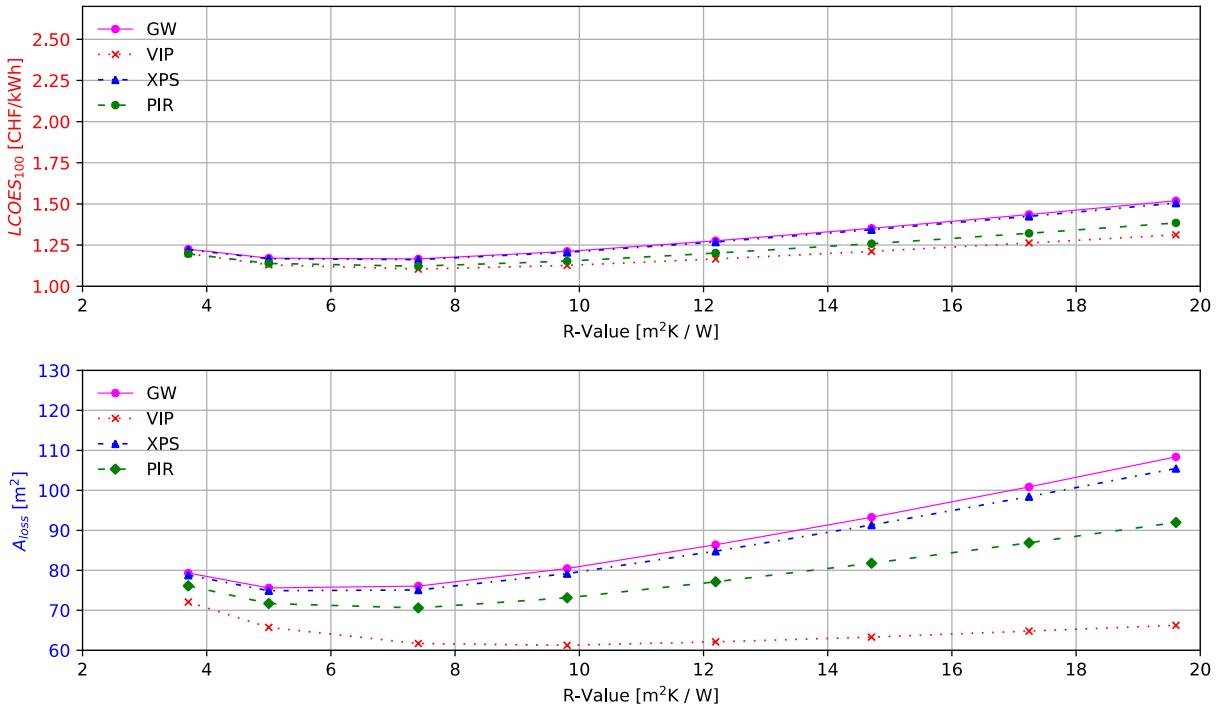

Fig. 34 – $LCOES_{100}$ and loss of living space (A_{loss}) as a function of R-value for each of the investigated thermal insulation materials. Scenario 1 (storage in building), retrofit case. Location: Bern.

Table 8 – Minimum $LCOES_{100}$ and corresponding loss of living space attained with each thermal insulation material (GW as baseline). Location: Bern. The values in parentheses indicate the relative cost and volume reduction achieved by changing the thermal insulation as compared to the baseline.

		GW	XPS	PIR	VIP
RF	$LCOES_{100}$ [CHF/kWh]	1.17	1.16 (1%)	1.12 (4%)	1.10 (6%)
	Living area loss [m²]	76	75 (1%)	71 (7%)	62 (18%)
	Optimum R-value [m²K/W]	7.41	7.41	7.41	7.41
NB-FA	$LCOES_{100}$ [CHF/kWh]	0.61	0.61 (0%)	0.60 (2%)	0.65 (–7%)
	Living area loss [m²]	76	75 (1%)	71 (7%)	66 (13%)
	Optimum R-value [m²K/W]	7.41	7.41	7.41	5.00
NB-FU	$LCOES_{100}$ [CHF/kWh]	0.37	0.38 (–3%)	0.39 (–5%)	0.44 (–19%)
	Living area loss [m²]	80	75 (6%)	71 (11%)	66 (18%)
	Optimum R-value [m²K/W]	9.80	7.41	7.41	5.00

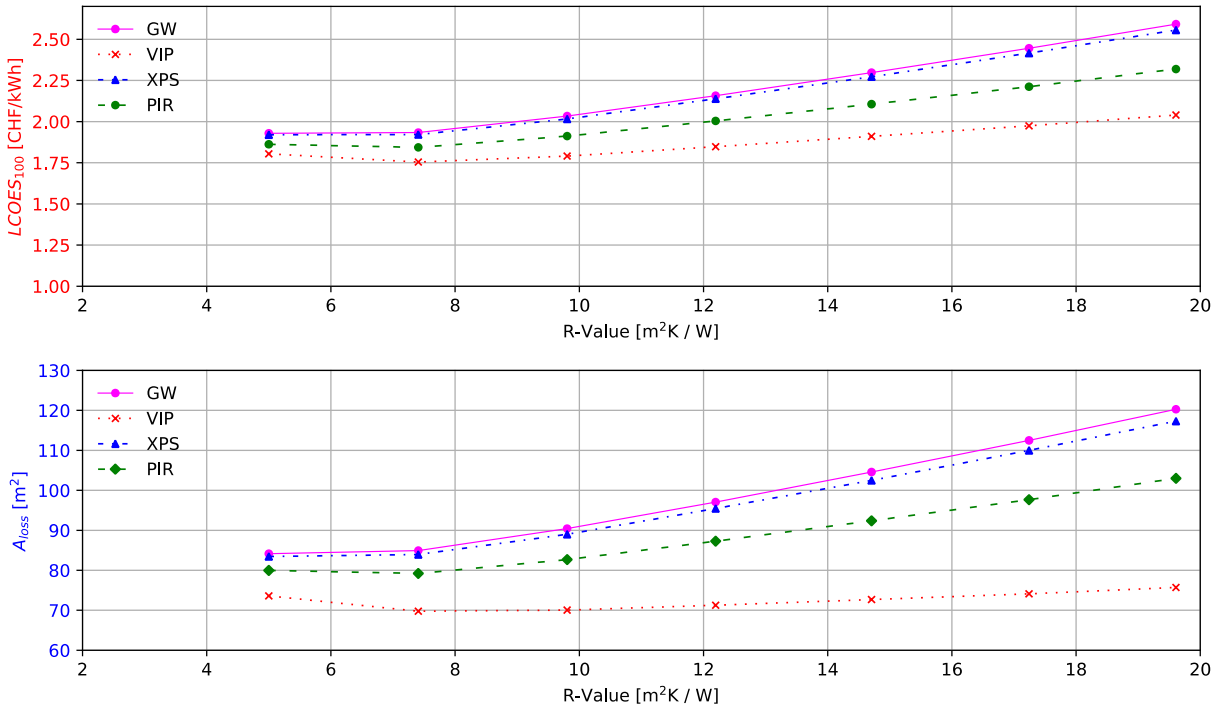

Fig. 35 – $LCOES_{100}$ and loss of living space (A_{loss}) as a function of R-value for each of the investigated thermal insulation materials. Scenario 1 (storage in building), retrofit case. Location: Zurich.

Table 9 – Minimum $LCOES_{100}$ and corresponding loss of living space attained with each thermal insulation material (GW as baseline). Location: Zurich. The values in parentheses indicate the relative cost and volume reduction achieved by changing the thermal insulation as compared to the baseline.

		GW	XPS	PIR	VIP
RF	$LCOES_{100}$ [CHF/kWh]	1.93	1.92 (1%)	1.84 (5%)	1.75 (9%)
	Living area loss [m²]	84	83 (1%)	79 (6%)	70 (17%)
	Optimum R-value [m²K/W]	5.00	5.00	7.41	7.41
NB-FA	$LCOES_{100}$ [CHF/kWh]	1.36	1.35 (1%)	1.31 (4%)	1.28 (6%)
	Living area loss [m²]	85	84 (1%)	79 (7%)	70 (18%)
	Optimum R-value [m²K/W]	7.41	7.41	7.41	7.41
NB-FU	$LCOES_{100}$ [CHF/kWh]	0.40	0.40 (0%)	0.41 (–2%)	0.47 (–18%)
	Living area loss [m²]	84	84 (0%)	79 (6%)	74 (12%)
	Optimum R-value [m²K/W]	7.41	7.41	7.41	5.00

6.6 Height of buried storage

The $LCOES_{100}$ of scenario 2, in which the storage is buried underground in direct vicinity of the building, is shown in Fig. 36. In Fig. 36, the blue curve (left axis) shows the minimum required storage volume, while the red curve (right axis) shows the calculated $LCOES_{100}$, both as a function of the tank height. Given that the heat losses in this case do not contribute to heating the building, the amount of energy to be provided to cover the SH demand is constant regardless of the tank configuration. The observed fluctuations in the storage volume are presumably the result of the different surface-to-volume ratios and the different dynamics within the storage due to the different heights (varying arrangement of the HEX and VES). By increasing the tank height from 7 to 15 m, the $LCOES_{100}$ is increased by approximately 20%. The reason for this significant increase is associated to the increased excavation costs (CHF/m^3) that results when a deeper excavation is required.

6.7 Comparison storage in building vs. buried underground

A final comparison is made to assess the economic potential of the vacuum-insulated storage buried underground as compared to the storage integrated inside the building. Both scenarios were simulated for Bern (value of real estate: 6'000 CHF/m^2) with the LFC (optimum controller identified in this work), α_{coll} = 45°, A_{coll} = 187 m^2, and the following parameters:

Scenario 1

- Storage integration: Inside the building
- V_{tank}: 180 m^3 (minimum to fulfill SH and DHW requirements)
- Tank height, h_{tank}: 15 m
- Thermal insulation: Glass wool ($\lambda_{ins} = 1.263 \cdot 10^{-4}T - 1.074 \cdot 10^{-3}$ W/mK)
- R-value: 7.4 m^{2}K/W (30 cm thickness)
- β: 0.5% (operational factor used to calculate OPEX)

Scenario 2

- Storage integration: Buried underground in direct vicinity of the building
- V_{tank}: 190 m^3 (minimum to fulfill SH and DHW requirements)
- Tank height, h_{tank}: 7 m
- Thermal insulation: Double-wall vacuum tank
- R-value: 20 m^{2}K/W
- β: 2.0% (operational factor used to calculate OPEX)

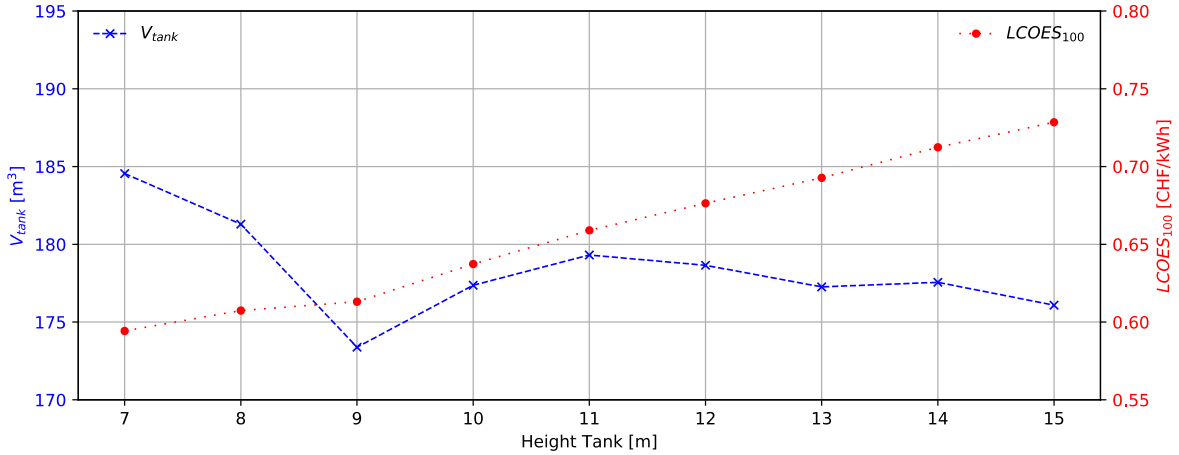

Fig. 36 – $LCOES_{100}$ and minimum required tank volume for scenario 2 (tank buried in the ground).

Table 10 – $LCOES_{100}$, $k_{VK,AF}$, OPEX and CAPEX for the two scenarios considered in this work. Scenario 1 (S1) includes the cases: retrofit (RT), new building with footprint affected (NB FA), new building with footprint unaffected (NB-FU). Here, $k_{VK,AF}$ represents the full annual costs (see Eq. 5-1).

	$LCOES_{100}$ [CHF/kWh]	**$k_{VK,AF}$** [CHF/a]	**OPEX** [CHF/a]	**CAPEX** [kCHF]	**OPEX / $k_{VK,AF}$** [%]
S1 RF	1.2	53'000	1'400	940'000	3
S1 NB-FA	0.6	27'000	1'400	455'000	5
S1 NB-FU	0.4	17'000	1'400	280'000	8
S2	0.6	26'000	5200	380'000	20

Table 10 shows a comparison of $LCOES_{100}$ and the various cost components for both scenarios. Scenario 1 (S1) further includes the cases: retrofit (RT), new building with footprint affected (NB-FA), new building with footprint unaffected (NB-FU). Given that the building has a self-sufficiency grade of 100%, the energy output of the storage (W in Eq. 5-1) equals the total annual energy demand for space heating and DHW. For the simulated system, W was round 44'000 kWh – out of it, the DHW requirement accounts for 48%.

As compared to the $LCOES_{100}$ attained in the retrofit case of scenario 1 (1.2 CHF/kWh), this study indicates that the option of a vacuum-insulated storage buried underground may halve the $LCOES_{100}$ (0.6 CHF/kWh) by avoiding the high penalty costs associated to the loss of living space and the internal reconstruction of the building. In the case NB-FA, both storage scenarios lead to very similar $LCOES_{100}$. In this case, the higher investment costs of S1 (mainly because of the high opportunity costs associated to the loss of potential living space) are compensated by the assumed higher operating costs of S2. Note that in calculating the $LCOES_{100}$, the OPEX has been assumed to be four times those of scenario 1, due to the lower TRL and increased complexity associated with the vacuum insulated storage technology. A 50% reduction in OPEX of S2 – which is expected to happen as the technology continues to mature – would allow reducing the $LCOES_{100}$ to 0.5 CHF/kWh. In the case NB-FU, the storage integrated inside the building seems to offer the most cost-effective solution ($LCOES_{100}$ ~ 0.4 CHF/kWh), however at the expense of additional heating the building during the summer season as a result of the unavoidable heat losses from the storage to its surroundings.

Fig. 37 shows a breakdown of the total investment costs (including costs associated to loss of living space) for both scenarios. The costs of components and their installation is virtually the same for all cases, given that the solar collector system is the same and cost of the storage (incl. its installation) only changes marginally between S1 (140 kCHF) and S2 (120 kCHF). Thus, the cost differences among the different cases are essentially driven by the following shares:

- S1 RF: loss of existing living space (480 kCHF, 51% of CAPEX)
- S1 NB-FA: loss of potential living space, i.e. opportunity costs (180 kCHF, 39% of CAPEX)
- S2: excavation costs (125 kCHF; 33% of CAPEX)

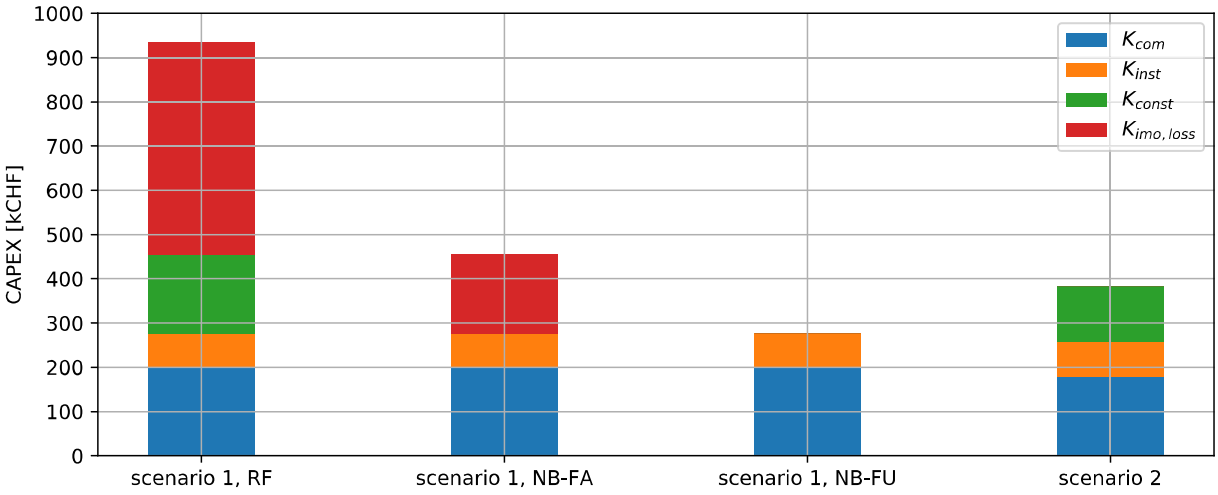

Fig. 37 – Breakdown of the total investment costs (CAPEX) for the two scenarios considered in this work. Scenario 1 further includes the cases: retrofit (RT), new building with footprint affected (NB-FA), new building with footprint unaffected (NB-FU). K_{com}: cost for storage and solar collectors; K_{ins}: cost for the installation of the storage and solar collectors; K_{const}: cost for the internal reconstruction of the building to integrate the storage (scenario 1) or cost for excavation of the soil (scenario 2).

7 Conclusions

Today, increasing market diffusion of STES requires reducing the high investment costs. In this work, a parametric-based optimization has been conducted to assess the potential of reducing the costs of hot-water STES through the use of alternative thermal insulation materials and an exergy-oriented control strategy of the solar collectors. The primarily goal of the study was the economic optimization of a STES system for retrofit applications – e.g. integration of the storage in an existing building. The investigated configurations included: (1) a hot-water thermally stratified storage tank, (2) a solar thermal collector installation, and (3) a multifamily low-energy building with a solar fraction of 100%. The analysis included the following thermal insulation materials: glass wool (GW), extruded polystyrene (XPS), polyurethane-polyisocyanurate foam (PUR-PIR), and vacuum insulation panels (VIP). The use of a vacuum-insulated storage tank (a double-wall tank with an evacuated envelope) was also evaluated as an alternative to avoid the integration of a large-volume storage inside a residential building.

The simulation-based analysis revealed that the required storage volume can be reduced by 30% by switching from a high-flow (baseline case) to a low-flow control strategy. A comparative analysis of the investigated controllers (high-flow, matched-flow, and low flow) revealed that the reason behind the specific performance characteristics of the given controllers directly correlate to the exergy distribution they effect within the storage. While the high-flow controller fails to replenish the high-temperature reserve of the storage during the winter season, the matched-flow controller leads to a strong thermal stratification and ultimately to the need of using the high-temperature reserve of the storage to cover the space heating demand – as a result, both controllers fail to satisfy the domestic hot water (DHW) demand. The low-flow controller, on the other hand, seemed to represent the ideal compromise between providing high-temperature heat for DHW and mid-temperature heat for the SH demand.

The simulation results indicate that increasing the solar tilt angle of the solar collectors from 45° (baseline) to an optimum of 65° can lead to a reduction in the storage volume of round 10%. If the hot-water tank is integrated as part of a retrofit case inside an existing residential building – where the costs are primarily driven by the loss of living space and the internal reconstruction of the building –, maximizing the solar collector area is the best strategy to minimize the Levelized Cost of Energy Storage ($LCOES_{100}$). In the retrofit scenario, vacuum-insulation panels (VIP) – as an alternative to conventional glass wool – can lead to 20% savings in living space and a cost advantage of about 5%. In general, the small cost benefit offered by VIP and PIR – as compared to glass wool – would probably not justify the additional complexities and uncertainties associated to these alternative materials. At an $LCOES_{100}$ of about 1.1 CHF/kWh, the integration of the storage inside an existing building is the most expensive option due to the high costs associated to the internal modification of the building and the loss of living space. The $LCOES_{100}$ can be reduced by 50% if the storage is integrated inside a new building – mainly because of the high building reconstruction costs that are avoided. If the regulations allow the storage to be removed from the calculation of the building footprint (in German the 'Ausnützungsziffer'), the $LCOES_{100}$ could be further reduced by 40%, reaching a minimum of 0.4 CHF/kWh.

As compared to the $LCOES_{100}$ attained in the retrofit case mentioned above (1.1 – 1.2 CHF/kWh), the outcome of this study indicates that the option of burying a vacuum-insulated tank underground might halve the $LCOES_{100}$ (0.6 – 0.7 CHF/kWh). Thus, commercially-available vacuum-insulated storages seem to be a promising solution for retrofit applications, as they offer the possibility of avoiding the high penalty costs associated to the loss of living space and the internal reconstruction of the building that is required when placing a large-volume tank inside an existing building. Moreover, a storage buried underground avoid the additional heating of the building during the summer season that results from the unavoidable heat losses from the storage to its surroundings.

8 National and international cooperation

At the national level, the motivation for this project arose from the collaboration between HSLU and Jenni Energietechnik AG. As a pioneering company in this field, Jenni Energietechnik AG provided valuable field data from their solar heated apartment buildings in Oberburg and important inputs that allowed the models developed in this work to be further refined. This collaboration led to discussions about the applicability of the project results, including the potential of applying the optimized solar control strategies in one of their existing solar heated buildings. The collaboration with Jenni Energietechnik AG will also extend over the coming years in the framework of the BFE project SensOpt[4]. The scope of SensOpt involves the detailed monitoring of a new solar heated apartment building in Huttwil, which is equipped with a seasonal thermal energy storage system provided by Jenni Energietechnik AG. SensOpt is conducted in close collaboration with SPF (Institute for Solar Technology, University of Applied Sciences Rapperswil), with whom information has been exchanged to ensure that the methodologies applied in both projects are consistent and that the results obtained from both projects are thereby directly comparable and complementary. Moreover, the findings of OPTSAIS – particularly those in relation to cost parameters and the optimized thermal insulation materials and control strategies – are expected to serve as a basis for the numerical study conducted in SensOpt.

An exchange between HSLU and LESBAT (Laboratory of Solar Energetics and Building Physics, School of Business and Engineering Vaud) has taken place to evaluate the possibility of actively pursuing and further developing the concept of the vacuum-insulated storage buried underground. LESBAT has assessed – in the framework of the BFE project VITES[5] – the technical feasibility of a double-wall vacuum insulated hot water thermal storage container. This initial collaboration may lead to a joint Innosuisse project. Also in relation to this concept, HSLU has been involved in the planning of a monitoring project of the Sonnenhaus Muttenz (www.sonnenhaus.swiss), where a vacuum-insulated storage is to be incorporated.

This project was also involved in the Swiss Competence Center for Energy Research “Heat and Electricity Storage” (SCCER HaE). The study and optimization of sensible seasonal thermal energy storage systems is embedded in one of the tasks of work package 1 of SCCER HaE. The funds provided by SCCER HaE allowed the detailed storage model used in this project to be developed. Through the SCCER, collaboration with scientists at ETH Zurich was set up in the fields of storage modeling and model predictive control. This initial collaboration lead to a joint publication and is expected to result in a joint research project to assess the potential of hybrid sensible/latent storages (water in combination with encapsulated phase change materials) for seasonal applications.

At the international level, the project has mainly involved the collaboration with the EU project Heat4Cool (www.heat4cool.eu). In the framework of this collaboration, OPTSAIS was able make use of the Heat4Cool modeling platform and the models already developed for the building and the solar thermal collector. Furthermore, the models for large/seasonal thermal energy stores will be a valuable contribution of HSLU for future European and national projects.

[4] SensOpt – Sensible saisonale Wärmespeicherung optimal eingesetzt für die vollständig solare Beheizung von Mehrfamilienhäusern. SFOE contract number: SI/501771-01

[5] VITES – Vacuum Insulated Thermal Energy Storage. SFOE contract number: SI/501691-01

9 Literature

[1] Hewicker C, Werner O, Ebert M, Mennel T, Verhaegh N, Raadschelders J. Energiespeicher in der Schweiz. Bedarf, Wirtschaftlichkeit und Rahmenbedingungen im Kontext der Energiestrategie 2050. 2013.

[2] Bundesamt für Energie Bern, Klemmer A, Piegsa A, Wüthrich P, Keller M, Jakob M, et al. Analyse des schweizerischen Energieverbrauchs 2000-2014 nach Verwendungszwecken. BFE 2015:66.

[3] Nationale Dienstleistungszentrale nDLZ Ernst Basler + Partner. Das Gebäudeprogramm im Jahr 2015, Jahresbericht 2015.

[4] Bundesamt für Statistik (BFS). Bau- und Wohnungswesen 2014. 2016.

[5] Gutschner M, Nowak S. Potenzialabschätzung zum solarthermischen Beitrag zur Wärmeversorgung im schweizerischen Wohngebäudepark. 2012.

[6] Gutschner M, Gnos S, Nowak S. Potenzialabschätzung für Sonnenkollektoren im Wohngebäudepark. 2010.

[7] Galli H. Josef Jenni packt die Sonne in den Tank. Der Bund 2013.

[8] Mangold, Dirk; Miedaner, Oliver; Tziggili, Ekaterini Pirmoudi; Schmidt, Thomas; Unterberger, Markus; Zeh B. Technisch-wirtschaftliche Analyse und Weiterentwicklung der Solaren Langzeit-Wärmespeicherung – Forschungsbericht zum BMU-Vorhaben 0329607N. Solites 2012.

[9] Hasnain SM. Review on sustainable thermal energy storage technologies, Part I: heat storage materials and techniques. Energy Convers Manag 1998;39:1127–38. doi:10.1016/S0196-8904(98)00025-9.

[10] Jenni Energietechnik AG - Energiespeicher in allen Grössen - Deutsch n.d. http://jenni.ch/home.html (accessed November 18, 2019).

[11] Energietechnik JA. Solarüberbauung Allmend, Huttwil. n.d.

[12] Langzeit-Wärmespeicher zum Energiesparen - Vakuum-Pufferspeicher n.d. https://vakuum-pufferspeicher.de/ (accessed November 18, 2019).

[13] Pufferspeicher Vakuumisoliert - sirch.com n.d. https://www.sirch.com/speicherbau/pufferspeicher-vakuumisoliert/ (accessed November 18, 2019).

[14] Solarenergie EE, Anwendungen V, Nussbaumer T, Sol MEE. Erneuerbare Energien – Solarenergie. 2019.

[15] Botpaev R, Louvet Y, Perers B, Furbo S, Vajen K. Drainback solar thermal systems: A review. Sol Energy 2016;128:41–60. doi:10.1016/j.solener.2015.10.050.

[16] SIA 385/1 (2009): Anlagen für Trinkwarmwasser in Gebäuden - Grundlagen und Anforderungen, Norm Ausgabe 2009 2011.

[17] Villasmil W, Fischer LJ, Worlitschek J. A review and evaluation of thermal insulation materials and methods for thermal energy storage systems. Renew Sustain Energy Rev 2019;103:71–84. doi:10.1016/j.rser.2018.12.040.

[18] EN 826:2013. Thermal insulating products for building applications - Determination of compression behaviour 2013.

[19] Koru M. Determination of Thermal Conductivity of Closed-Cell Insulation Materials That

Depend on Temperature and Density. Arab J Sci Eng 2016;41:4337–46. doi:10.1007/s13369-016-2122-6.

[20] Ochs F, Heidemann W, Müller-Steinhagen H. Effective thermal conductivity of moistened insulation materials as a function of temperature. Int J Heat Mass Transf 2008;51:539–52. doi:10.1016/j.ijheatmasstransfer.2007.05.005.

[21] Abdou AA, Budaiwi IM. Comparison of Thermal Conductivity Measurements of Building Insulation Materials under Various Operating Temperatures. J Build Phys 2005;29:171–84. doi:10.1177/1744259105056291.

[22] Dominguez-Munoz F, Anderson B, Cejudo-Lopez JM, Carrillo-Andres A. Uncertainty in the thermal conductivity of insulation materials. Energy Build 2010;42:2159–68. doi:10.1016/j.enbuild.2010.07.006.

[23] Abdou A, Budaiwi I. The variation of thermal conductivity of fibrous insulation materials under different levels of moisture content. Constr Build Mater 2013;43:533–44. doi:10.1016/j.conbuildmat.2013.02.058.

[24] Omer SA, Riffat SB, Qiu G. Thermal insulations for hot water cylinders: a review and a conceptual evaluation. Build Serv Eng Res Technol 2007;28:275–93. doi:10.1177/0143624406075269.

[25] Baetens R, Jelle BP, Thue JV, Tenpierik MJ, Grynning S, Uvsløkk S, et al. Vacuum insulation panels for building applications: A review and beyond. Energy Build 2010;42:147–72. doi:10.1016/j.enbuild.2009.09.005.

[26] Cuce E, Cuce PM, Wood CJ, Riffat SB. Toward aerogel based thermal superinsulation in buildings: A comprehensive review. Renew Sustain Energy Rev 2014;34:273–99. doi:10.1016/j.rser.2014.03.017.

[27] Kalnæs SE, Jelle BP. Vacuum insulation panel products: A state-of-the-art review and future research pathways. Appl Energy 2014;116:355–75. doi:10.1016/j.apenergy.2013.11.032.

[28] Pfundstein M, Gellert R, Spitzner MH, Rudolphi A. Insulating Materials: Principles, Materials, Applications. vol. 8504. 1st ed. 2008.

[29] Riffat SB, Qiu G. A review of state-of-the-art aerogel applications in buildings. Int J Low-Carbon Technol 2013;8:1–6. doi:10.1093/ijlct/cts001.

[30] Wong JCH, Kaymak H, Brunner S, Koebel MM. Mechanical properties of monolithic silica aerogels made from polyethoxydisiloxanes. Microporous Mesoporous Mater 2014;183:23–9. doi:10.1016/j.micromeso.2013.08.029.

[31] Miros A, Psiuk B, Szpikowska-Sroka B. Aerogel insulation materials for industrial installation: properties and structure of new factory-made products. J Sol-Gel Sci Technol 2017;84:496–506. doi:10.1007/s10971-017-4539-0.

[32] Jelle BP. Traditional, state-of-the-art and future thermal building insulation materials and solutions - Properties, requirements and possibilities. Energy Build 2011;43:2549–63. doi:10.1016/j.enbuild.2011.05.015.

[33] Papadopoulos AM. State of the art in thermal insulation materials and aims for future developments. Energy Build 2005;37:77–86. doi:10.1016/j.enbuild.2004.05.006.

[34] Al-Homoud MS. Performance characteristics and practical applications of common building thermal insulation materials. Build Environ 2005;40:353–66. doi:10.1016/j.buildenv.2004.05.013.

[35] Zhang H, Fang WZ, Li YM, Tao WQ. Experimental study of the thermal conductivity of

polyurethane foams. Appl Therm Eng 2017;115:528–38. doi:10.1016/j.applthermaleng.2016.12.057.

[36] Winterling H, Sonntag N. Rigid polystyrene foam (EPS, XPS). Kunststoffe Int 2011;101:18–21.

[37] Gnip I, Vėjelis S, Vaitkus S. Thermal conductivity of expanded polystyrene (EPS) at 10°C and its conversion to temperatures within interval from 0 to 50°C. Energy Build 2012;52:107–11. doi:10.1016/j.enbuild.2012.05.029.

[38] Karamanos A, Hadiarakou S, Papadopoulos AM. The impact of temperature and moisture on the thermal performance of stone wool. Energy Build 2008;40:1402–11. doi:10.1016/j.enbuild.2008.01.004.

[39] Yue DT, Tan ZC, Di YY, Lv XR, Sun LX. Specific heat capacity and thermal conductivity of foam glass (type 150P) at temperatures from 80 to 400 K. Int J Thermophys 2006;27:270–81. doi:10.1007/s10765-006-0026-5.

[40] Ventrella A, Smeacetto F, Salvo M, Ferraris M. Characterization of new glass coated foam glass insulating tiles by standard tests. J Mater Eng Perform 2012;21:2380–8. doi:10.1007/s11665-012-0164-9.

[41] Yatsenko EA, Goltsman BM, Smolii VA, Kosarev AS. Foamed slag glass - Eco-friendly insulating material based on slag waste. 2015 IEEE 15th Int Conf Environ Electr Eng EEEIC 2015 - Conf Proc 2015;0124:819–23. doi:10.1109/EEEIC.2015.7165270.

[42] Tereshchenko IM, Dormeshkin OB, Kravchuk AP, Zhikh BP. Status and Prospects of Development of Production of Glassy Foamed Heat-Insulation Materials. Glas Ceram (English Transl Steklo i Keramika) 2017;74:216–9. doi:10.1007/s10717-017-9965-5.

[43] Pittsburgh Corning. Product Profile, FOAMGLAS Buliding 2018. https://uk.foamglas.com/-/media/ukfoamglascom/alle-dokumente/building/downloads/documentation/135-pb0915_produkteprofil-pcuk_2016_f_foamglas_medium.pdf (accessed July 31, 2018).

[44] Schuetz P, Scoccia R, Gwerder D, Waser R, Sturzenegger D, Elguezabal P, et al. Fast simulation platform for retrofitting measures in residential heating. CCHAVC, 2018.

[45] Schuetz P, Scoccia R, Gwerder D, Waser R, Sturzenegger D, Elguezabal P, et al. Fast assessment platform for energy consumption of different configurations in residential heating with thermal storages. Enerstock 2018, Çukurova Univ., 2018.

[46] Rahman A, Smith AD, Fumo N. Performance modeling and parametric study of a stratified water thermal storage tank. Appl Therm Eng 2016;100:668–79. doi:10.1016/j.applthermaleng.2016.01.163.

[47] VDI-Wärmeatlas, 11. Auflage. n.d.

[48] Industry PC for A and R. Glythermin ○IT P 44 1999.

[49] Haller M, Ruschenburg J, Ochs F, Bony J, Dott R. The Reference Framework of System Simulations of the IEA SHC Task 44/HPP Annex 38 - Part A: General Simulation Boundary Conditions. Tech Rep Subtask C IEA SHC Task 44 2013.

[50] Perez R, Ineichen P, Seals R, Michalsky J, Stewart R. Modeling Daylight availability and irradiance components from direct and global irradiance 1990;44:271–89.

[51] Wemhöner C, Hafner B, Schwarzer K. Simulation of Solar Thermal Systems With Carnot Blockset. Proc. Eurosun 2000 Conf. ISES, Copenhagen, Denmark, 2000, p. 1–6.

[52] Endress Hauser. Coriolis Massflow Sensor F300. n.d.

[53] Bundesamt für Statistik (BFS). Bau- und Wohnungswesen, Gebäude n.d.

https://www.bfs.admin.ch/bfs/de/home/statistiken/bau-wohnungswesen/gebaeude.html (accessed June 1, 2018).

[54] Kanton Bern. Bauverordnung (BauV) 2017. https://www.belex.sites.be.ch/frontend/versions/923 (accessed June 1, 2018).

[55] Kanton Zürich. Planungs- und Baugesetz (PBG) 2018. https://www.zh.ch/internet/de/rechtliche_grundlagen/gesetze/erlass.html?Open&Ordnr=700.1 (accessed June 1, 2018).

[56] Bundesamt für Statistik (BFS). Allgemeine Übersicht “Gebäude” nach Kantonen 2016 n.d. https://www.bfs.admin.ch/bfs/de/home/statistiken/bau-wohnungswesen/gebaeude.assetdetail.6286264.html (accessed June 1, 2018).

[57] BFE. Bau- und Wohnungswesen 2017 - Bau- und Wohnbaustatistik 2017, Gebäude- und Wohnungsstatistik 2017, Leerwohnungszählung vom 1. Juni 2018 | Publikation n.d. https://www.bfs.admin.ch/bfs/de/home/statistiken/bau-wohnungswesen.assetdetail.7966565.html (accessed November 19, 2019).

[58] Vereinigung Kantonaler Feuerversicherungen VKF. Brandschutzvorschriften 2015 2017. https://www.bsvonline.ch/de/vorschriften/ (accessed June 1, 2018).

[59] SIA 385/2 (2014): Anlagen für Trinkwarmwasser in Gebäuden - Warmwasserbedarf, Gesamtanforderungen und Auslegung, Norm Ausgabe 2014 2014.

[60] Jordan U, Vajen K. Tool for the Generation of Domestic Hot Water (DHW) Profiles on a Statistical Basis Version 1.10. DHWcal Man Version 202b 2017;10:1–14.

[61] Bundesamt für Meteorologie und Klimatologie. Wetter Daten n.d. https://www.meteoschweiz.admin.ch/home.html?tab=overview.

[62] Intro - Meteonorm (de) n.d. https://meteonorm.com/ (accessed November 19, 2019).

[63] En K, Ergebnisse T, Keymark-zertifikat AS, F S. Summary of EN 12975 Test Results , annex to Solar KEYMARK Certificate a tu st re o Annual collector output based on EN 12975 Test Results , annex to Solar KEYMARK Certificate 011-7 S1834 F Annual collector output kWh / Jährliche Kollektor Leistung kWh / E 2011:9–10.

[64] Harmonisierung der Baubegriffe Leitfaden. 2017.